

Theory and modeling of molecular modes in the NMR relaxation of fluids[†]

Thiago J. Pinheiro dos Santos,¹ Betül Orcan-Ekmeçci,² Walter G. Chapman,¹ Philip M. Singer,¹ and Dilipkumar N. Asthagiri³

¹*Department of Chemical and Biomolecular Engineering, Rice University, Houston, Texas 77005, USA.*

²*Department of Mathematics, Rice University, Houston, Texas 77005, USA.*

³*Oak Ridge National Laboratory, Oak Ridge, Tennessee 37830, USA.*

(*Electronic mail: asthagiridn@ornl.gov)

(*Electronic mail: ps41@rice.edu)

(Dated: 9 January 2024)

Traditional theories of the NMR autocorrelation function for intramolecular dipole pairs assume single-exponential decay, yet the calculated autocorrelation of realistic systems display a rich, multi-exponential behavior resulting in anomalous NMR relaxation dispersion (i.e., frequency dependence). We develop an approach to model and interpret the multi-exponential autocorrelation using simple, physical models within a rigorous statistical mechanical development that encompasses both rotational and translational diffusion in the same framework. We recast the problem of evaluating the autocorrelation in terms of averaging over a diffusion propagator whose evolution is described by a Fokker-Planck equation. The time-independent part admits an eigenfunction expansion, allowing us to write the propagator as a sum over modes. Each mode has a spatial part that depends on the specified eigenfunction, and a temporal part that depends on the corresponding eigenvalue (i.e., correlation time) with a simple, exponential decay. The spatial part is a probability distribution of the dipole-pair, analogous to the stationary states of a quantum harmonic oscillator. Drawing inspiration from the idea of inherent structures in liquids, we interpret each of the spatial contributions as a specific molecular mode. These modes can be used to model and predict NMR dipole-dipole relaxation dispersion of fluids by incorporating phenomena on the molecular level. We validate our statistical mechanical description of the distribution in molecular modes with molecular dynamics simulations interpreted without any relaxation models or adjustable parameters: the most important poles in the Padé-Laplace transform of the simulated autocorrelation agree with the eigenvalues predicted by the theory.

[†]Notice: This manuscript has been authored by UT-Battelle, LLC, under contract DE-AC05-00OR22725 with the US Department of Energy (DOE). The US government retains and the publisher, by accepting the article for publication, acknowledges that the US government retains a nonexclusive, paid-up, irrevocable, worldwide license to publish or reproduce the published form of this manuscript, or allow others to do so, for US government purposes. DOE will provide public access to these results of federally sponsored research in accordance with the DOE Public Access Plan (<http://energy.gov/downloads/doe-public-access-plan>).

I. INTRODUCTION

Atomic nuclei with non-zero spin magnetic moment ($I \geq 1/2$) can be excited and driven out of equilibrium by a resonating radio-frequency electromagnetic radiation in the presence of an external magnetic field B_0 . When the radio-frequency perturbation is removed, the relaxation of the spins back to the initial equilibrium with B_0 provides important insights into the structure and behavior of matter. This process of nuclear magnetic resonance (NMR) relaxation has thus emerged as a powerful tool in probing matter non-destructively, with applications spanning hydrocarbon recovery to material science¹⁻³. It is known that the NMR relaxation at different frequencies $\omega_0 = \gamma B_0$ (a.k.a., NMR relaxation dispersion) is governed by phenomena at different length and time scales^{3,4}. The NMR dipole-dipole relaxation that is of interest here – either “like spins” (e.g., ^1H - ^1H pairs) or “unlike spins” (e.g., ^{13}C - ^1H pairs, or alternatively e^- - ^1H pairs) – is sensitively dependent on the translational and rotational diffusion of the species in the system. Further, since the perturbation by the external applied field is small relative to thermal energies, it is possible to use the unperturbed Hamiltonian of the system to model the evolution of the system and then use that information to study

the NMR relaxation. Molecular dynamics (MD) simulations have proven successful in predicting NMR dipole-dipole relaxation of bulk, viscous, and confined fluids in good to excellent agreement with experiments for both like spins⁵⁻¹¹ and unlike spins (at high frequencies)^{12,13}, all without using adjustable parameters to interpret the simulations or by coarse-graining the dynamics. Besides us, other groups have also presented compelling studies exploring NMR relaxation using molecular simulations¹⁴⁻²⁶.

The original theory of intramolecular NMR relaxation, due to Bloembergen, Purcell, and Pound (BPP)²⁷, assumes that relaxation arises from the rotational diffusion of the molecule. BPP assumed that the molecules behaved as hard-spheres and their rotational motion in the liquid was random. By estimating the rotational correlation time τ_d based on an extension of Debye’s theory of dielectric dispersion, BPP predicted that the NMR autocorrelation function $G(t)$ for dipole pairs decays mono-exponentially, resulting in a specific functional form (namely, a Lorentzian) for NMR relaxation dispersion. From early on, it was well-appreciated that the BPP model or its derivatives were oversimplified, and efforts were made to address the shortcomings²⁸⁻³². In practice, however, to circumvent the shortcomings it is more common to construct an empirical (i.e., phenomenological) model for the

NMR relaxation dispersion, such as the Kohlrausch-Williams-Watts function³³, Cole-Davidson function³⁴ or Lipari-Szabo³⁵ model for like spins, or, the extended Solomon-Bloembergen-Morgan model^{36–38} for unlike spins.

Meanwhile, Torrey³⁹ addressed the role of translational diffusion on intermolecular NMR relaxation by using a random walk model. This led to a single characteristic translational relaxation time τ_T to be associated with the diffusion correlation time τ_D . Later, Hwang and Freed improved Torrey's model by taking the structure of the fluid into account⁴⁰; specifically, they considered a hard-sphere fluid or a dilute electrolyte for which models of pair-correlations are available.

Woessner took the pioneering first steps to understand the role of molecular conformations to induce multi-exponential behavior. He studied the diffusional motion of spherical and ellipsoidal objects within which the magnetic dipoles (of either fixed or varying separation and orientation) were embedded^{41,42}. Woessner attributed the multiple correlation times to different internal conformations, although by construction his formalism would be restricted to a few discrete configurations^{28,41–43}. Steele used a classical mechanical approach to model molecular reorientations, specifically by modeling the torque on molecules by a constant friction plus a random contribution^{4,29,44}. A different approach based on using an analytical diffusion propagator was successfully applied to derive pulsed gradient spin-echo attenuation equations⁴⁵, NMR relaxation under anomalous diffusion⁴⁶, and relaxation of dipole pairs in planar^{3,47}, cylindrical^{3,45}, and spherical pores^{3,45,47,48} with different boundary conditions.

In our earlier studies, instead of fitting the NMR autocorrelation function $G(t)$ to an empirical model with adjustable parameters, we sought to expand $G(t)$ for the case of regular diffusion into multiple "modes"

$$G(t) = \int_0^\infty \exp\left(-\frac{t}{\tau}\right) P(\tau) d\tau, \quad (1)$$

where each "mode" τ has a mono-exponential decay and $P(\tau)$ is the probability density distribution of the time constants of the "modes". The intuition guiding this approach was that there are inherent dynamical structures in the fluid that define each mode. Note also that with such an expansion, the NMR relaxation dispersion is given by BPP-like terms weighted by $P(\tau)$, and can potentially give physical insights into how specific molecular motions affect relaxation.

In this work, we establish a theoretical framework for the expansion (Eq. 1) and derive a clearer physical meaning into the "modes." To this end, we describe the NMR relaxation between two dipoles using classical statistical mechanics. Instead of assuming discrete characteristic conformations, we solve the Fokker-Planck equation to obtain the phase distribution function, from which we calculate the autocorrelation function $G(t)$ and NMR relaxation dispersion. For specific cases, we can obtain analytical solutions and these turn out to obey the multi-exponential behavior defined above. We use MD simulations to validate the theory and guide the physical interpretation of the simulation results. For dipoles that are constrained to remain at a fixed separation, the multi-exponential behavior collapses into a mono-exponential be-

havior, in agreement with the traditional BPP theory.

II. THEORY

Let us assume two dipoles undergoing relaxation in the presence of an external magnetic field B_0 in a viscous fluid. For convenience, we fix the first dipole at the center of the coordinates, and the other dipole is free to move around the first. The NMR autocorrelation function $G^m(t)$ resulting from fluctuating magnetic fields of dipole pairs is given by^{5,12,49}

$$G^m(t) = \left\langle \frac{Y_2^m(\theta(t), \phi(t))}{r^3(t)} \frac{Y_2^m(\theta(0), \phi(0))}{r^3(0)} \right\rangle, \quad (2)$$

where $\theta(t)$ and $\phi(t)$ are the angles formed by the two magnetic dipoles and the external magnetic field B_0 . A constant factor depending on the spins has been suppressed for clarity. We will return to this in the Section III, Simulation Methodology. Y_2^m is the spherical harmonic of degree 2, $r(t)$ is the distance between particles I and S . For isotropic systems, as is the case in this work, $G^m(t)$ is independent of the order m , which is equivalent to saying that the direction of the applied static magnetic field B_0 is arbitrary. Without loss of generality, we therefore choose to compute only the $m = 0$ case, and from here on refer only to $G(t)$ where $m = 0$ is implied. Also, in the following, for concision, we will use $Y_2^0(t) \equiv Y_2^0(\theta(t), \phi(t))$.

The Fourier transform of $G(t)$, for different Larmor frequencies $\omega_0 = \gamma B_0$, gives the spectral density function $J(\omega)$ through the relationship⁵

$$J(\omega) = 2 \int_0^\infty G(t) \cos(\omega t) dt, \quad (3)$$

which is used to calculate the relaxation times T_1 and T_2 at different NMR frequencies $\omega_0 = \gamma B_0$, a.k.a. relaxation dispersion, for like spins⁹ or unlike spins¹³.

The auto-correlation in Eq. (2) can be obtained once we know the diffusion propagator

$$\rho(\mathbf{r}, \mathbf{r}_0, t) = \rho(\mathbf{r}, t | \mathbf{r}_0, 0) p(\mathbf{r}_0), \quad (4)$$

for the probability of traversing \mathbf{r}_0 to \mathbf{r} in time t ; here, $\mathbf{r} = \{r, \theta, \phi\}$ (in spherical coordinates). Notice that $p(\mathbf{r}_0)$ is the prior probability of the initial state, where $\rho(\mathbf{r}, t | \mathbf{r}_0, 0)$ is the transition probability^{1,45}. In the NMR literature, $\rho(\mathbf{r}, t | \mathbf{r}_0, 0)$ is also referred as the diffusion propagator or the Green function^{3,50}. Observe that the quantity $\rho(\mathbf{r}, \mathbf{r}_0, t)$ is hence a phase probability density function, and $\rho(\mathbf{r}, \mathbf{r}_0, t) d\mathbf{r} d\mathbf{r}_0$ is the joint probability of having the dipole with configuration \mathbf{r}_0 in $d\mathbf{r}_0$ initially and with configuration \mathbf{r} in $d\mathbf{r}$ at any time t ¹.

Once $\rho(\mathbf{r}, \mathbf{r}_0, t)$ is available, we can rewrite the ensemble average in Eq. (2) as an integration over the diffusion propagator as^{1,50}

$$G(t) = \int d\mathbf{r} \int d\mathbf{r}_0 \frac{Y_2^0(t)}{r^3(t)} \frac{Y_2^0(0)}{r^3(0)} \rho(\mathbf{r}, \mathbf{r}_0, t), \quad (5)$$

where, $d\mathbf{r} = r^2 \sin \theta dr d\theta d\phi$ (and likewise for $d\mathbf{r}_0$), and the limits of integration over r or r_0 ranges from r_i (the initial radial location) to r_f (the final radial location).

The evolution of $\rho(\mathbf{r}, \mathbf{r}_0, t)$ can be described by the Fokker-Planck equation^{40,45,51}, in the form that already assumes the fluctuation–dissipation theorem. For notational simplicity, denoting $\rho(\mathbf{r}, t) \equiv \rho(\mathbf{r}, \mathbf{r}_0, t)$, we have

$$\frac{\partial}{\partial t} \rho(\mathbf{r}, t) = \nabla^2 [D\rho(\mathbf{r}, t)] - \nabla \cdot \left[\rho(\mathbf{r}, t) \frac{D}{k_B T} F(\mathbf{r}, t) \right], \quad (6)$$

where D is the diffusion coefficient of the bulk fluid (i.e., without confinement), k_B is the Boltzmann constant, T is temperature, and $F(\mathbf{r}, t)$ is the force acting on the second dipole. Here we assume the Einstein-Smoluchowski relation for the friction forces acting on the dipole⁵². For the particular case of a stationary potential of interaction $U(\mathbf{r})$ between the dipoles, we know that

$$F(\mathbf{r}, t) = -\nabla U(\mathbf{r}), \quad (7)$$

which allows us to rewrite Eq. (6) as

$$\frac{\partial}{\partial t} \rho(\mathbf{r}, t) = \nabla^2 [D\rho(\mathbf{r}, t)] + \nabla \cdot \left[\rho(\mathbf{r}, t) \frac{D}{k_B T} \nabla U(\mathbf{r}) \right]. \quad (8)$$

$$G(t) = \int d\mathbf{r} \int d\mathbf{r}_0 \frac{Y_2^0(t)}{r^3(t)} \frac{Y_2^0(0)}{r^3(0)} \exp \left[-Dt\nabla^2 + \frac{Dt}{k_B T} \nabla \cdot (\nabla U(\mathbf{r})) \right] \rho(\mathbf{r}, 0). \quad (10)$$

Notice that explicit time dependence only appears in the exponential factor, which then emphasizes that $G(t)$ can be represented by the generic form

$$G(t) = \sum_{k=1}^{\infty} P(\tau_k) \exp \left(-\frac{t}{\tau_k} \right), \quad (11)$$

in which each characteristic correlation time $\tau_k = \tau_k(r, \theta, \phi, r_0, \theta_0, \phi_0)$. However, except for very simple cases, the analytical transformation from Eq. (10) to Eq. (11) is non-trivial. Further, $P(\tau)$ can be multi-modal. However, in principle, each mode with characteristic time τ contains key information about the structure and the dynamics of the system.

It is worth emphasizing here that for the case of ^1H NMR relaxation of water in biological cells, Brownstein and Tarr had already identified that a multi-exponential time decay of the NMR magnetization $M(t)$ arises as a consequence of an eigenvalue problem, which is dependent on the size, shape, and surface relaxivity of the cells³⁰. Further advances were also made in the literature^{45,53–55}. Although our formalism is independent from these works, and furthermore our formalism addresses the NMR autocorrelation function $G(t)$ rather than the NMR magnetization decay $M(t)$, the fact that we obtained similar conclusions regarding the arising of multi-exponential decays supports the multi-eigenvalue approach for NMR relaxation in general.

In the following sections, we will employ the idea of solving for the phase distribution function $\rho(\mathbf{r}, t)$ and finding the corresponding NMR autocorrelation function $G(t)$ for dipole

This equation should be solved subject to periodic boundary conditions $\rho(r, \theta, \phi, t) = \rho(r, \theta, \phi + 2\pi, t)$, proper radial boundary conditions for the inner radius r_i and outer radius r_f , impenetrability condition $\rho(0, \theta, \phi, t) = 0$, and initial condition $\rho(r, \theta, \phi, 0) = p(r_0, \theta_0, \phi_0)$. At this point, we observe that we can express the solution to the problem in terms of the matrix exponential operator

$$\rho(\mathbf{r}, t) = \exp \left[-Dt\nabla^2 + \frac{Dt}{k_B T} \nabla \cdot (\nabla U(r, \theta, \phi)) \right] \rho(\mathbf{r}, 0). \quad (9)$$

where $\rho(\mathbf{r}, 0)$ is the initial distribution. Substituting Eq. (9) into Eq. (5), we have

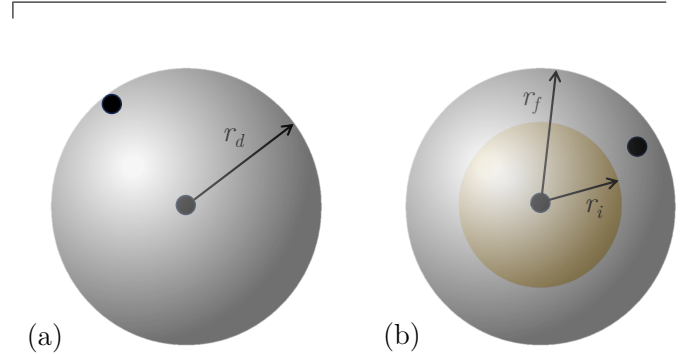


FIG. 1. Configuration of the two magnetic dipoles in which (a) they are separated by a constant distance r_d (discrete spherical shell) and (b) they are separated by a non-constant distance bounded by an inner radius r_i and an outer radius r_f (thick spherical shell)

pairs. This will also enable analytical expressions for the underlying distribution $P(\tau)$ of molecular modes of relaxation.

A. Fixed distance and non-interacting dipoles

Consider first two non-interacting dipoles at fixed separation r_d (Figure 1(a)). For convenience, we fixed one of the dipoles at the center of coordinates, and we aim to solve for the phase distribution function of the second dipole with respect to the central one.

In spherical coordinates, $\mathbf{r}_d = \{r_d, \theta, \phi\}$, $U(\mathbf{r}_d) = 0$, and

thus Eq. (8) can be written as

$$\frac{\partial}{\partial t} \rho(\mathbf{r}_d, t) = D \left[\frac{1}{r_d^2 \sin \theta} \frac{\partial}{\partial \theta} \left(\sin \theta \frac{\partial}{\partial \theta} \right) + \frac{1}{r_d^2 \sin^2 \theta} \frac{\partial^2}{\partial \phi^2} \right] \rho(\mathbf{r}_d, t). \quad (12)$$

where D is a diffusion coefficient of the dipole. We assume normal diffusion, i.e. D is a constant. The initial condition of the mobile dipole is

$$\rho(\mathbf{r}_d, 0) = \frac{\delta(\theta - \theta_0) \delta(\phi - \phi_0)}{\sin \theta} p(\mathbf{r}_{d,0}), \quad (13)$$

where $p(\mathbf{r}_{d,0})$ is the probability of having that initial discrete position, $\mathbf{r}_{d,0}$. Further, for an isotropic system, the system obeys periodicity in θ and ϕ , and then one can show that

$$\rho(\mathbf{r}_d, t) = \frac{1}{4\pi} Y_2^0(t) Y_2^0(0) \exp\left(-\frac{6Dt}{r_d^2}\right). \quad (14)$$

Using this result in Eq. (5) without integrating over the constant r_d , and by the orthogonality of the spherical harmonics, we obtain that

$$G(t) = \frac{1}{4\pi r_d^6} \exp\left(-\frac{6Dt}{r_d^2}\right). \quad (15)$$

This result is simply the mono-exponential decay from the traditional BPP theory and has been derived in different ways^{1,37}. Additional details of the analytical solution are given in the Supplementary Information. Finally, observe from Eq. (15) that the characteristic time for this mono-exponential decay is given by

$$\tau_d = \frac{r_d^2}{6D}, \quad (16)$$

and, after restoring the constant factors from Eq. (2), the corresponding amplitude can be obtained by identifying the second moment contribution to $G(t)$ at $t = 0$, such that

$$P(\tau_d) = \frac{1}{4\pi r_d^6}. \quad (17)$$

B. Non-fixed distance and non-interacting dipoles

Having established the result for a simple, well-known case, we next consider the case where the two dipoles are not at fixed distance. Hence, we must now account for the radial diffusion between an inner radius $r = r_i$ and an outer radius $r = r_f$ (Figure 1(b)). This accounts for the changes in the distance between the dipoles due to sampling of different molecular conformation (for the case of intramolecular relaxation) and thermal fluctuations, and thus compared to the BPP-model, adds an additional degree of freedom to the dipoles. This model can be an approximate description of ^1H - ^1H interactions on the two extremes of a long hydrocarbon chain for the case of like-spins, or the relaxation of ^1H

from water molecules in the inner-shell of paramagnetic ions for the case of unlike-spins. It is important to clarify that our formalism only accounts for rotational diffusion in the polar and azimuthal directions and translational diffusion along the radial axis. We emphasize that we do not model the translational exchange between the inner-shell and the bulk with respect to the central dipole, as in the Hwang-Freed model⁴⁰.

Therefore, now Eq. (8) can be written by

$$\frac{\partial}{\partial t} \rho(\mathbf{r}, t) = D \left[\frac{1}{r^2} \frac{\partial}{\partial r} \left(r^2 \frac{\partial}{\partial r} \right) + \frac{1}{r^2 \sin \theta} \frac{\partial}{\partial \theta} \left(\sin \theta \frac{\partial}{\partial \theta} \right) + \frac{1}{r^2 \sin^2 \theta} \frac{\partial^2}{\partial \phi^2} \right] \rho(\mathbf{r}, t). \quad (18)$$

Assuming isotropy, we have periodicity in θ and ϕ ; further, we use Neumann (reflecting) boundary conditions

$$\left. \frac{\partial \rho(r, \theta, \phi, t)}{\partial r} \right|_{r=r_i} = 0, \quad (19)$$

$$\left. \frac{\partial \rho(r, \theta, \phi, t)}{\partial r} \right|_{r=r_f} = 0.$$

The initial condition of the mobile dipole is given by

$$\rho(\mathbf{r}, 0) = \frac{\delta(r - r_0) \delta(\theta - \theta_0) \delta(\phi - \phi_0)}{r^2 \sin \theta} p(\mathbf{r}_0), \quad (20)$$

where $p(\mathbf{r}_0)$ is the probability of having that initial discrete position.

For the above conditions, the time-dependent equilibrium distribution function is given by

$$\rho(\mathbf{r}, t) = \frac{3}{4\pi(r_f^3 - r_i^3)} Y_2^0(t) Y_2^0(0) \sum_{k=1}^{\infty} \frac{j_2(\lambda_{2,k} r_0) j_2(\lambda_{2,k} r)}{N_{2,k}} \exp(-\lambda_{2,k}^2 D t), \quad (21)$$

where $j_2(\lambda_{2,k} r)$ is the 2nd-order spherical Bessel function of the first kind, and $N_{2,k}$ is the normalization constant that arises from orthogonality of spherical Bessel functions assuming Neumann boundary conditions, i.e.,⁵⁶

$$\int_{r_i}^{r_f} j_2(\lambda_{2,i} r) j_2(\lambda_{2,k} r) r^2 dr = N_{2,k} \delta_{ik},$$

$$N_{2,k} = \frac{r^3}{2} \left(1 - \frac{6}{(r \lambda_{2,k})^2} \right) j_2(\lambda_{2,k} r) \Big|_{r=r_i}^{r=r_f}. \quad (22)$$

In order to satisfy the Neumann boundary conditions and having in mind the result from Eq. (21), the only possible values of $\lambda_{2,k}$ are those that satisfy the corresponding Sturm-Liouville eigenvalue problem (SL-EVP)⁵⁷, which is given by

$$j'_n(\lambda_{2,k} r_i) y'_n(\lambda_{2,k} r_f) - y'_n(\lambda_{2,k} r_i) j'_n(\lambda_{2,k} r_f) = 0, \quad (23)$$

where the prime indicate derivatives with respect to r . The eigenvalues $\lambda_{2,k}$ will be the positive roots of equation above,

allowing the solution in Eq. (21) to be expanded in terms of their corresponding eigenfunctions⁵⁸. Here, we ignore the trivial solution $\lambda_{2,k} = 0$. Notice that the eigenvalues depend on the functional form of the Eq. (23), which is a consequence of the boundary condition, and on the values of r_i and r_f .

For simplicity, because it is implied that only the second moments are of interest to NMR relaxation, we simplified the notation for the eigenvalues from $\lambda_{2,k}$ to λ_k . Using the result in Eq. (5) and integrating over all possible coordinates in the system, and using the orthogonality of spherical harmonics, we find

$$G(t) = \frac{3}{4\pi(r_f^3 - r_i^3)} \sum_{k=1}^{\infty} \exp(-\lambda_k^2 D t) \int_{r_i}^{r_f} \int_{r_i}^{r_f} \frac{1}{rr_0} \frac{j_2(\lambda_k r) j_2(\lambda_k r_0)}{N_{2,k}} dr dr_0. \quad (24)$$

It is important to highlight a couple of points about the result in Eq. (24). Firstly, we observe that now the NMR autocorrelation function has a multi-exponential decay, which comes as an infinite set of discrete characteristic decay times that depend on the corresponding eigenvalues. Secondly, we must recall that Eq. (24) should be computed under the definition of the inner-product (orthogonality) in Eq. (22) that arise from the boundary conditions, such that the calculated quantities are projected into the correct orthogonal eigenfunction set. The detailed derivation can be found in the Supplementary Information.

Eq. (24) shows that the characteristic time for the k^{th} -mode is

$$\tau_k = \frac{1}{\lambda_k^2 D} \quad k = 1, 2, \dots, \infty \quad (25)$$

and, after restoring the constant factors from Eq. (2), the corresponding amplitude (second moment contribution to the autocorrelation function at $t = 0$) is

$$P(\tau_k) = \frac{3}{4\pi(r_f^3 - r_i^3)} \sum_{k=1}^{\infty} \int_{r_i}^{r_f} \int_{r_i}^{r_f} \frac{1}{rr_0} \frac{j_2(\lambda_k r) j_2(\lambda_k r_0)}{N_{2,k}} dr dr_0. \quad (26)$$

III. SIMULATION METHODOLOGY

We performed molecular simulations using LAMMPS⁵⁹ to address the systems covered in our theoretical formulation. We have adopted two types of reduced units in this work: Lennard-Jones (LJ) reduced units for the simulation parameters, and NMR reduced units for the calculation of relaxation rates.

Consider first the LJ reduced units. The relationships between real (denoted by \dagger) and LJ-reduced quantities are defined for quantities like mass (M), distance (r), time (t), frequency (ω), temperature (T), and molecular friction constant

(f) by

$$\begin{aligned} M &= \frac{M^\dagger}{m}, \\ r &= \frac{r^\dagger}{\sigma}, \\ t &= t^\dagger \sqrt{\frac{\epsilon}{m\sigma^2}}, \\ \omega &= \omega^\dagger \sqrt{\frac{m\sigma^2}{\epsilon}}, \\ T &= \frac{T^\dagger k_B}{\epsilon}, \\ f &= f^\dagger \sqrt{\frac{\sigma^2}{m\epsilon}}. \end{aligned} \quad (27)$$

In our simulation, LJ-particles with $m = 1.0$ (a.u.), $\epsilon = 0.1$ (a.u.), and $\sigma = 0.1$ (a.u.) carry the dipoles. Usually LJ-reduced quantities are represented by (*), but we omit this for simplicity.

Next consider NMR reduced units. The dimensionless (i.e., reduced) NMR relaxation rates ($1/T_{1,2}$) are related to real units $1/T_{1,2}^\dagger$ ($time^{-1}$) by

$$\frac{1}{T_{1,2}} = \frac{1}{T_{1,2}^\dagger} \frac{\sigma^6}{\alpha} \sqrt{\frac{\epsilon}{m\sigma^2}}, \quad (28)$$

where the constant α ($time^{-2} \times distance^6$) is generally given by

$$\alpha = \frac{4\pi}{5} \left(\frac{\mu_0}{4\pi}\right)^2 \hbar^2 \gamma_I^2 \gamma_S^2 S(S+1), \quad (29)$$

wherein μ_0 is the vacuum permittivity, \hbar is the modified Planck's constant ($\hbar = h/2\pi$), and γ_I and γ_S are the gyromagnetic ratios for particles with spin I and S , respectively. For like spins, $\gamma_I = \gamma_S$ and $I = S$. In this equation, the ‘‘measured’’ dipole has spin I and gyromagnetic ratio γ_I , while the ‘‘influencing’’ dipole has spin S and gyromagnetic ratio γ_S . Alternatively, α can be included in the definition of $G^m(t)$ in Eq. 2 as a multiplicative factor. Without loss of generality, we set $\alpha = 1$ for NMR reduced units.

In our simulations, we use a cut-off distance $r_c = 0.1$ always less than the minimum distance between the dipoles in the simulation box to ensure they do not interact. For simplicity, the first dipole was kept at the center of the simulation box, while the second dipole was constrained in the annulus (Figure 1(b)) by LJ-WCA walls⁶⁰. We use Langevin dynamics with different friction constants f to propagate the dynamics, and a timestep of $\delta t = 0.0001$ while sampling the configurations every 100 timesteps (the configuration sampling rate is $\delta t_{samp} = 0.01$). The friction constant f (in Langevin dynamics) is related to the diffusion coefficient D of the dipoles by

$$D = \frac{k_B T}{f}, \quad (30)$$

where $k_B = 1$ is Boltzmann's constant in LJ-reduced units. Note that we define D as the diffusion coefficient for the bulk

fluid (i.e., without confinement), which is time independent and normally defined as “ D_0 ” in porous media.

It is important to highlight that LJ-reduced units imply the use of the corresponding states law, i.e., the solution in LJ-reduced units can be converted to any physical systems of interest given that appropriate LJ-parameters for the system are known (m , ε , and σ). Overall, the results obtained with such LJ-reduced units are broad and general.

We calculate the autocorrelation function $G(t)$ from the MD trajectory using in-house codes after rewriting Eq. (2) as

$$G(t) = \frac{5}{16\pi} \left\langle \frac{(3 \cos^2 \theta(t+t') - 1)}{r^3(t+t')} \frac{(3 \cos^2 \theta(t') - 1)}{r^3(t')} \right\rangle_{t'} \quad (31)$$

where t' is the lag-time, and the indexes I and S refer to the measured and influencing dipole in the dipole pair, respectively. Recall from Eq. (2) that $G(t)$ is the normalized autocorrelation function.

A. Padé-Laplace inversion recovery

As shown in the theoretical development, given that dipoles undergoing NMR relaxation under normal diffusion yield a multi-exponential decay, we can write the $G(t)$ from molecular simulations as

$$G(t) = \sum_{j=1}^n P(\mu_j) \exp(-\mu_j t), \quad (32)$$

where n is the number of exponential decays, and $P(\mu_j)$ is the amplitude (probability) for a mode with decay-rate μ_j . The Laplace transform of $G(t)$ is given by⁶¹

$$L(p) = \int_0^\infty \exp(-pt) G(t) dt, \quad (33)$$

$$L(p) = \sum_{j=1}^n \frac{P(\mu_j)}{p - \mu_j}. \quad (34)$$

Eq. 34 makes it clear that the number of exponential decays is the same as the number of poles of the Laplace transform. We seek the Padé approximant $R_{n-1,n}(p)$ of $L(p)$ ⁶². That is, we seek

$$L(p) = R_{n-1,n}(p) = \frac{A_{n-1}(p)}{B_n(p)}, \quad (35)$$

in which $A_{n-1}(p)$ is a polynomial of order $n-1$ and $B_n(p)$ is a polynomial of order n . The left-hand side of equation (35) can be expanded in a Taylor series about a point p_0 , where a good choice for p_0 is the inverse of the time necessary for $G(t)$ to decay to half of its initial value. Therefore,

$$d_0 + d_1(p - p_0) + \dots + d_{2n-1}(p - p_0)^{2n-1} = \frac{a_0 + a_1(p - p_0) + \dots + a_{n-1}(p - p_0)^{n-1}}{1 + b_1(p - p_0) + \dots + b_n(p - p_0)^n}, \quad (36)$$

where the Taylor series coefficients $d_0, d_1, \dots, d_{2n-1}$ are given by

$$d_i = \frac{1}{i!} \left(\frac{d^{(i)}L}{dp^{(i)}} \right)_{p=p_0}. \quad (37)$$

These coefficients can be calculated using numerical integration of the derivatives of equation (33) by

$$\begin{aligned} d_i \frac{i!}{\Delta t} = \frac{1}{2} & [(-t_0)^i \exp(-p_0 t_0) G(0) \\ & + (-t_{M-1})^i \exp(-p_0 t_{M-1}) G(M-1)] \\ & + \sum_{j=1}^{M-2} (-t_j)^i \exp(-p_0 t_j) G(j). \end{aligned} \quad (38)$$

Finally, we can get the coefficients of the Padé approximants $A_{n-1}(p)$ and $B_n(p)$ from the Taylor expansion coefficients. We then perform a partial fraction decomposition of $R_{n-1,n}(p) = \frac{A_{n-1}(p)}{B_n(p)}$ using MATLAB⁶³, returning a sum of fractions as in equation (34). By analyzing the magnitude of the numerator of these partial fractions, we can determine the amplitude and also the number of poles N that are physical^{61,62}. In practice, the number of poles is determined by trying different orders of Padé approximants starting from $n = 1$ up to the point $n = N + 1$ when no more new physical poles are identified. As we add more physical poles, we are in effect constructing better models of $P(\tau)$. Thus, one could envision using a maximum entropy (MaxEnt) approach to determine when to cutoff the process of adding new physical poles. We plan to investigate this approach in future studies. Here we include all the physical poles.

If needed, the final physical poles and corresponding amplitudes from this inversion were refined using a standard Particle Swarm Optimization (PSO) procedure to improve the adjustment to the simulation data⁶⁴. We have presented the agreement between the original NMR dipole-dipole autocorrelation from MD simulations and its corresponding reconstructed signal through the Padé-Laplace inversion in the Supplementary Information.

IV. RESULTS AND DISCUSSION

A. Fixed distance and non-interacting dipoles

For the case of fixed distance and non-interacting dipoles, we have seen from Eq. (15) that the NMR autocorrelation function $G(t)$ has a single molecular mode (mono-exponential decay) with characteristic time τ_d given by Eq. (16) and the corresponding amplitude $P(\tau_d)$ given by Eq. (17). Since this result holds for isotropic systems, this mode is known for being a simple rotational diffusion component. Figure 2 shows the comparison of the MD simulation NMR relaxation modes recovered with the Padé-Laplace method, and the theoretical results predicted from equations Eqs. (16) and (17). We observe excellent agreement between simulations and theory across different LJ-reduced distances r_d at constant friction

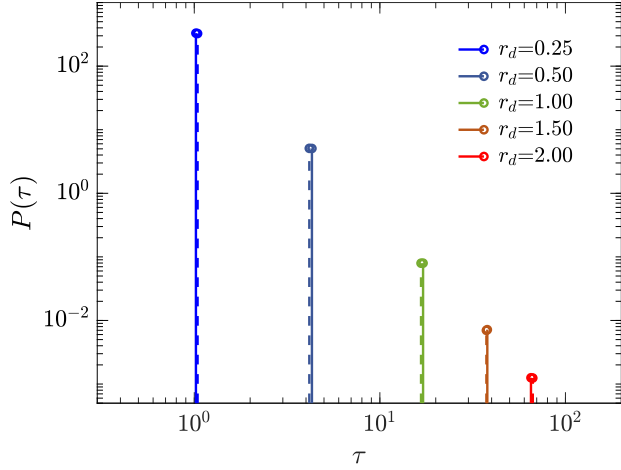


FIG. 2. Molecular modes of NMR relaxation in LJ-reduced units for dipole pairs at different fixed distances r_d , with constant friction $f = 100$ and $T = 1.00$. The solid lines represent the theoretical predictions, while the dashed lines represent the MD simulation results.

$f = 100$ and $T = 1.00$. To contextualize these parameters, we can give the example of liquid water⁶⁵ ($m = 3.0103 \times 10^{-26}$ kg, $\sigma = 2.725 \times 10^{-10}$ m, $\varepsilon = 4.9115 \times 10^{-21}$ J). Thus, the temperature in real units would correspond to $T^\dagger = 358.38$ K and $f^\dagger \propto 10^{-12}$ kg/s with $D^\dagger \propto 10^{-9}$ m²/s, which is within the typical range of diffusion coefficients for liquids.

Figure 3 shows a comparison of (LJ-reduced) characteristic relaxation times from MD simulations and the theoretical predictions across different LJ-reduced friction constants f at constant distance $r_d = 1.00$ and $T = 1.00$. For water as an example, this would correspond to $r^\dagger = 2.725$ Å or about one water molecular diameter, with diffusion coefficients $D^\dagger \propto 10^{-8} - 10^{-9}$ m²/s, as is typical for liquids. We again observe excellent agreement, showing that the characteristic relaxation time increases with the increment of the molecular friction in the system, but its amplitude remains the same. Physically, this confirms that the magnitude of the NMR relaxation rate depends solely on the distance between the fixed dipoles, but the characteristic time of the rotational diffusion mode increases as the viscous forces increase in the system, i.e., when the dipole diffusion decreases.

Finally, we calculate the spin-lattice $1/T_1(\omega)$ and spin-spin $1/T_2(\omega)$ relation rates in the low frequency limit ($\omega_0 = 0$) for the case of like-spins. Given that $1/T_1(0) = 1/T_2(0) = 1/T_{1,2}(0)$ in the zero frequency limit, we show that

$$\frac{1}{T_{1,2}(0)} = 5J(0) = 10G(0)\tau_d \quad (39)$$

in which $J(0)$ is the spectral density in Eq. 3. The real units $1/T_{1,2}^\dagger$ can be deduced from Eq. 28 and Eq. 29 where α can be calculated with $\gamma_I = \gamma_S$ and $I = S$ for the case of like spins.

The results of $T_{1,2}$ for both MD simulations and theory are summarized in Table I for the two dipoles at different fixed distances, and in Table II for the two dipoles at fixed distance

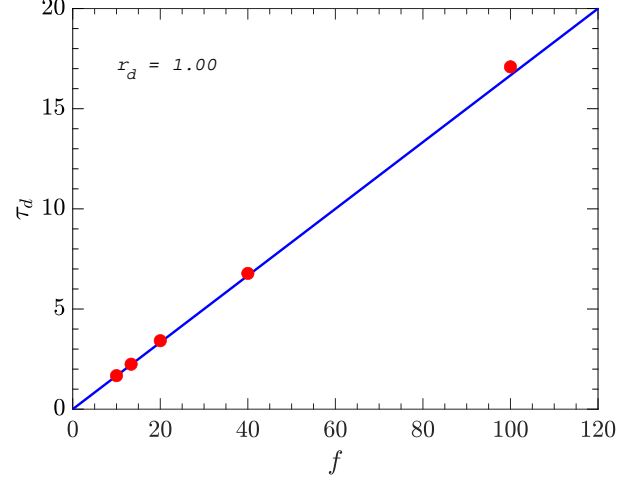


FIG. 3. LJ-reduced characteristic time τ_d of NMR relaxation for dipole pairs with different friction constants f , at $r_d = 1.00$ and $T = 1.00$. The solid line represent the theoretical predictions, while the solid points represent the MD simulation results.

but different friction constants. Overall, the agreement obtained for the data serves as a validation for the MD simulations.

r_d	$1/T_{1,2}(0)$	
	MD simulations	Theory
0.25	3367.8 ± 191.1	3395.3
0.50	218.3 ± 14.2	212.2
1.00	13.6 ± 1.2	13.3
1.50	2.7 ± 0.3	2.6
2.00	0.8 ± 0.1	0.8

TABLE I. Reduced relaxation rate $1/T_{1,2}(0)$ at zero frequency for two dipoles at different r_d , with $f = 100$ and $T = 1.00$.

f	$1/T_{1,2}(0)$	
	MD simulations	Theory
10.0	1.4 ± 0.1	1.3
13.3	1.8 ± 0.1	1.8
20.0	2.7 ± 0.1	2.7
40.0	5.4 ± 0.4	5.3
100.0	14.3 ± 1.2	13.3

TABLE II. Reduced relaxation rate $1/T_{1,2}(0)$ at zero frequency for two dipoles at different f , with $r_d = 1.00$ and $T = 1.00$.

B. Non-fixed distance and non-interacting dipoles

For the case when one of the dipoles is free to move in the annulus, as noted above we must find a multi-exponential (hence, multi-mode) decay. From Eq. (24), we find that each characteristic time τ_k is given by Eq. (25), and the corresponding amplitude $P(\tau_k)$ is given by Eq. (26). Notice that the amplitude $P(\tau_k)$ of each mode τ_k depends on the eigenvalue λ_k and the geometry of the system defined by the inner radius r_i and the outer radius r_f . Further, the integral needs to be calculated whilst observing the definition of the inner-product (orthogonality) in Eq. (22) that depends on the boundary conditions.

Figures 4(a) and 4(b) show the $P(\tau_k)$ distribution for two systems with spherical shell thickness limited by $r_f = 2.00$ and (a) with $r_i = 0.75$ and (b) with $r_i = 1.10$. In both cases, we employed $f = 10$ and $T = 1.0$. For water as an example, these distances correspond to $r_i^\dagger \approx 2.0 - 5.5 \text{ \AA}$ (from a fraction of the size of water to two water molecule diameters), the physical temperature is roughly $T^\dagger = 358.38 \text{ K}$, and $f^\dagger \propto 10^{-11} \text{ kg/s}$ with $D^\dagger \propto 10^{-8} \text{ m}^2/\text{s}$, as expected for liquids. Two key features stand out. First, it is worth noticing that MD simulations do capture the multi-exponential behavior, but usually the shorter modes *are not* captured because (i) $\tau_k \leq \delta t_{\text{samp}} = 0.01$, the sampling time for configurations, hindering the Padé-Laplace method from detecting such short modes, and/or (ii) the amplitudes of these modes small enough to be swamped by simulation noise (low signal to noise ratio). Recalling that the summation of all the amplitudes $P(\tau_k)$ should equal $G(0)$, it is interesting to notice that the simulation results *fold in* the effect of the un-captured shorter modes within the first two main captured modes, increasing their amplitudes to satisfy the correct $G(0)$. Second, we notice from Figures 4(a) and 4(b) that there is an inversion in the amplitude between the first and second largest modes. By keeping $r_f = 2.00$ constant, the second mode τ_2 presents a higher amplitude than τ_1 in the case where $r_i = 0.75$, while an opposite behavior is observed for $r_i = 1.10$. The physical significance of these modes will be further explored later.

Figures 5 and 6 show respectively the τ_k values and their corresponding $P(\tau_k)$ across different spherical thickness as a function of the ratio r_i/r_f , keeping $r_f = 2.00$ constant. Again, $f = 10$ and $T = 1.0$ in all cases. For simplicity, only the theoretical results up to $k = 3$ were shown. Observe from Figure 5 that the curves for τ_k never cross each other, signifying that these characteristic relaxation times are never degenerate, as expected. In Figure 6, the dotted line encompass a region where not all the points can be calculated with high numerical accuracy given our approximated numerical approach that uses the regular definition of inner-product (Euclidean space). This dotted region represent a monotonic curved based on interpolation of points computed within acceptable numerical accuracy in that region given the deviations from the regular Euclidean space and the non-euclidean space defined by the inner-product and orthogonality condition in Eq. (22). More details about the numerical criteria and the interpolation can be found in the Supplementary Information. Overall, the agreement between MD simulation results and the theo-

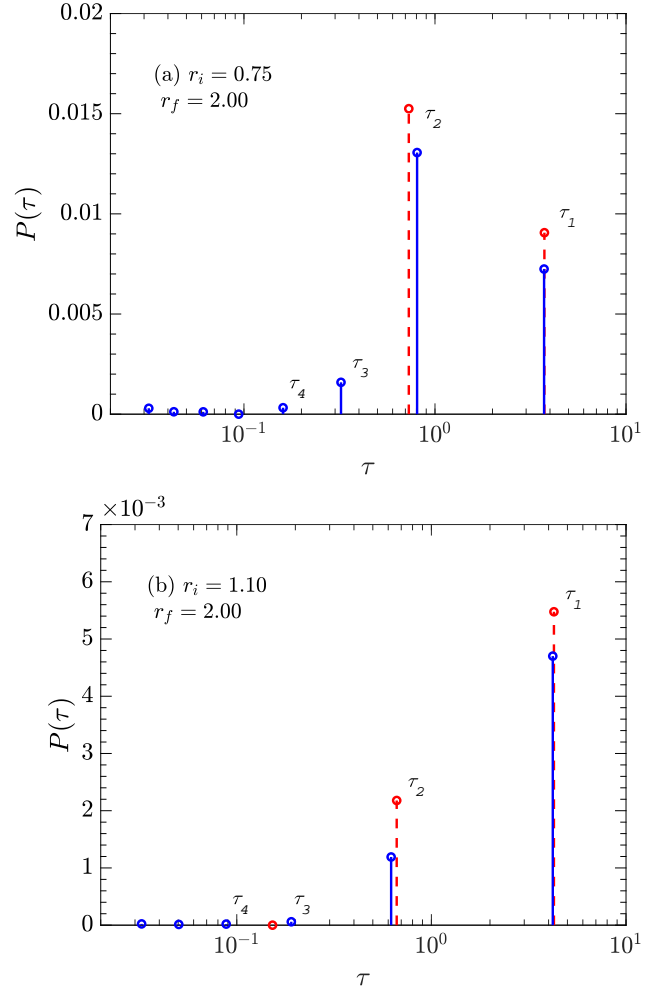


FIG. 4. Molecular modes of NMR relaxation in LJ-reduced units for dipole pairs at non-fixed distances for the case of (a) $r_i = 0.75$ and $r_f = 2.00$ and (b) $r_i = 1.10$ and $r_f = 2.00$, with constant friction $f = 10$ and $T = 1.00$. The solid lines represent the theoretical predictions, while the dashed line represents the MD simulation results.

retical predictions is satisfactory and supports our formalism. Moreover, it is important to analyze how the theory behaves in the limiting cases where $r_i/r_f \rightarrow 1$ and $r_i/r_f \rightarrow 0$.

When $r_i/r_f \rightarrow 1$, the thickness of the spherical shell is zero and the dipoles are at fixed distances, and a single exponential decay (single mode) will be expected in the system according to the traditional BPP theory. Observe from Figures 5 and 6 that when $r_i/r_f \rightarrow 1$, the theory predicts that τ_1 will have a non-zero finite value, with also a non-zero finite corresponding amplitude $P(\tau_1)$. On the other hand, all the remaining modes ($k = 2, 3, \dots, \infty$) shorten to zero in this limit, with a corresponding amplitude that also converges to zero. Moreover, the values of τ_1 and $P(\tau_1)$ predicted by our solutions match the expected BPP values in this limit.

When $r_i/r_f \rightarrow 0$, the two dipoles are so close that any small relative motion will affect the angular terms that drive NMR relaxation (Eq. (31)) within a very short time, meaning that

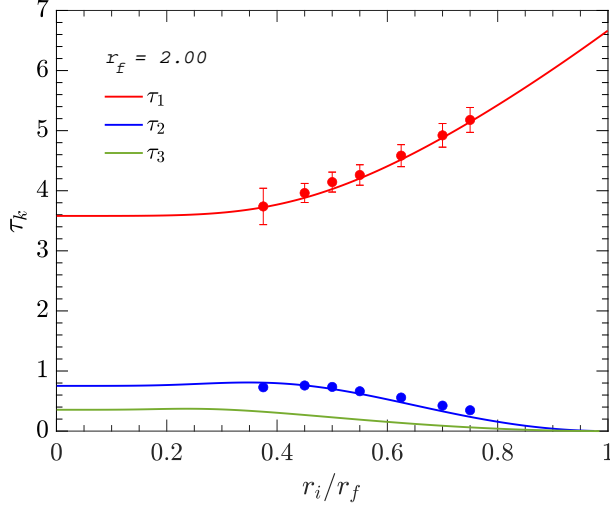


FIG. 5. Molecular modes LJ-reduced characteristic times τ_k up to the third largest mode as a function of r_i/r_f , for the case of $r_f = 2.00$ with $f = 10$ and $T = 1.0$. The solid lines represent the theoretical predictions, while the solid points represent the MD simulation results.

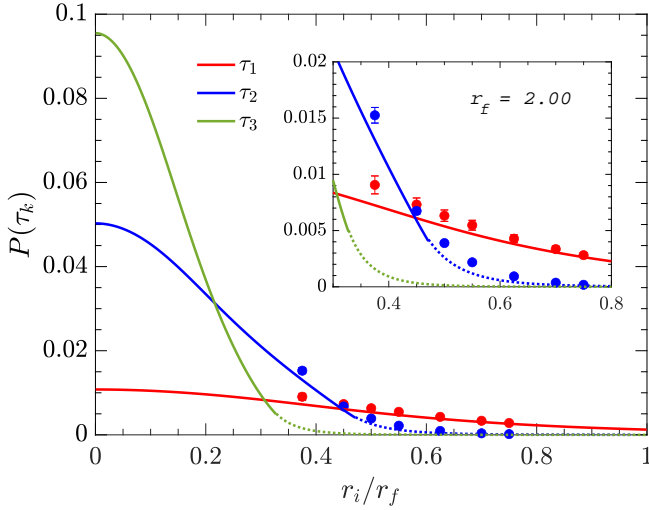


FIG. 6. Molecular modes amplitudes $P(\tau_k)$ up to the third largest mode as a function of r_i/r_f , for the case of $r_f = 2.00$ with $f = 10$ and $T = 1.0$. The solid lines represent the theoretical predictions, while the solid points represent the MD simulation results. The dotted lines are the interpolation of the theoretical predictions between points of higher numerical integration accuracy.

shorter characteristic time modes will play a bigger role than longer ones. The actual limit $r_i/r_f = 0$ is non-physical, since the two dipoles cannot occupy the same point in space. Observe from Figures 5 and 6 that, as we approach $r_i/r_f \rightarrow 0$, the theory predicts that all τ_k will have a non-zero finite value, with a non-zero finite amplitude $P(\tau_k)$ that grows as k increases, i.e., $P(\tau_{k+1}) > P(\tau_k)$. Overall, the fact that our analytical results make physical sense in the limiting cases of

r_i/r_f , together with the agreement with MD simulations for intermediate r_i/r_f cases, supports our theoretical solution.

By combining Eqs. (25) and (30), and recognizing that the Langevin friction parameter f has an Arrhenius-like temperature dependence⁶⁶, we can write that

$$\tau_k = \frac{f}{\lambda_k^2 k_B T} \propto \frac{A}{\lambda_k^2 k_B T} \exp\left(\frac{E_A}{k_B T}\right), \quad (40)$$

where A is a pre-exponential Arrhenius parameter, and E_A is the associated activation energy in LJ-reduced units. Notice that Eq. (40) clarifies the temperature dependence of each of these characteristic times τ_k . Firstly, we observe that this temperature dependence does not strictly follow an Arrhenius behavior, but for high enough temperatures, the temperature dependence of τ_k will follow an Arrhenius-like behavior. A similar conclusion has been made empirically for the case of ^1H of water relaxing on the inner-shell hydration around a paramagnetic ion, in which an Arrhenius-like behavior was observed for the temperature dependence of the molecular modes of the system¹³.

Similarly to the constant radius case, we also estimate $1/T_1(0) = 1/T_2(0) = 1/T_{1,2}(0)$ in the zero frequency limit ($\omega_0 = 0$) for like spins, such that

$$\frac{1}{T_{1,2}(0)} = 10 G(0) \langle \tau \rangle = 10 \sum_k P(\tau_k) \tau_k. \quad (41)$$

Note that even though a distribution in correlation times $P(\tau_k)$ exists (which leads to a multi-exponential decay of the auto-correlation function $G(t)$), the observed (i.e., measured) relaxation rate $1/T_{1,2}$ in Eq. 41 is single valued, resulting in a single-exponential decay of the observed magnetization $M(t)$.

Figure 7 illustrates good agreement between the theoretical predictions for $1/T_{1,2}(0)$ and the results from MD simulations. We have provided in the Supplementary Information a percentage breakdown of the contribution from different molecular modes to the relaxation rate $1/T_{1,2}(0)$ over different ranges of r_i/r_f . We find that the first mode contributes to 100% of $1/T_{1,2}(0)$ at $r_i/r_f = 1$, as expected in the BPP limit. However, the contribution from the first mode to $1/T_{1,2}(0)$ decreases to $\simeq 71\%$ at $r_i/r_f = 0.375$ (for example), with the remaining $\simeq 29\%$ coming from higher order modes ($k \geq 2$).

C. Analysis of the NMR dispersion

The $1/T_1(\omega_0)$ dispersion can also be computed from the distribution in modes $P(\tau_k)$, for either like spins¹¹ or unlike spins¹³. For the case of like spins, one can show that¹¹

$$\frac{1}{T_1(\omega_0)} = 2 \sum_k P(\tau_k) \left[\frac{\tau_k}{1 + (\omega_0 \tau_k)^2} + \frac{4\tau_k}{1 + (2\omega_0 \tau_k)^2} \right], \quad (42)$$

In the Supplementary Information we provide the expression for the case of unlike spins.

We know that, in general, for any $r_i/r_f (< 1)$, the contribution of the first mode to $1/T_1(\omega_0)$ will monotonically decrease with increasing frequency when $\omega_0 \tau_1 \gtrsim 1$. Thus, as

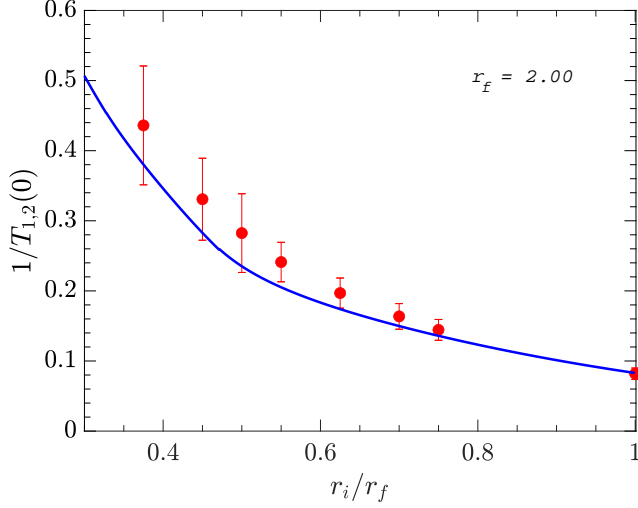


FIG. 7. Reduced relaxation rate $1/T_{1,2}$ at $\omega_0 = 0$ (i.e., the zero frequency limit) for different r_i/r_f , with $r_f = 2.00$, $f = 10$ and $T = 1.0$. The solid line represents the theoretical prediction, while the solid points represent the MD simulation results. We have also included the MD simulation result in the limit of $r_i/r_f \rightarrow 1$, which is the limit of fixed distance dipoles.

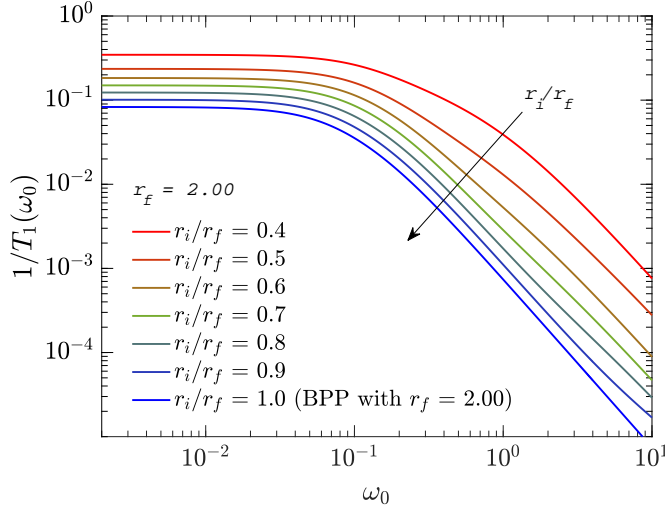


FIG. 8. Reduced relaxation rate $1/T_1$ dispersion as a function of the frequency ω_0 for different r_i/r_f , with $r_f = 2.00$, $f = 10$ and $T = 1.0$.

the frequency ω_0 increases, the importance of higher order modes also increase. Figure 8 shows the NMR dispersion for $1/T_1(\omega_0)$ for different values of r_i/r_f . This plot includes modes up to $k = 4$, which for cases studied here allow the determination of $1/T_1$ up to $\omega_0 = 10$. For higher ω_0 , more modes will be required. This result confirms that, as the thickness of the annulus increases (r_i/r_f decreases), higher order modes play a bigger role and increase $1/T_1$. Meanwhile, $1/T_2(\omega_0)$ shows only minor dispersion.

Figure 9 presents the NMR dispersion for $1/T_1(\omega_0)$ normalized by the corresponding zero frequency limit, i.e.,

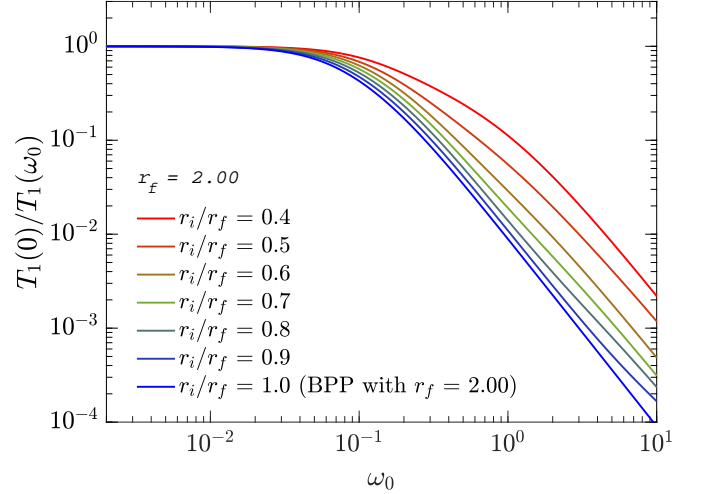


FIG. 9. Reduced relaxation rate $1/T_1$ dispersion normalized by the corresponding zero frequency limit $1/T_1(0)$ for different r_i/r_f , with $r_f = 2.00$, $f = 10$ and $T = 1.0$.

$T_1(0)/T_1(\omega_0)$. The plot includes the case $r_i/r_f = 1$, which is equivalent to the BPP limit where $1/T_1(\omega_0) \propto \omega_0^{-2}$ at high frequencies. For $r_i/r_f < 1$, however, deviations from BPP arise at high frequencies including modified power-law and non power-law dispersion. This signifies that the BPP model for $G(t)$ is not sufficient for $r_i/r_f < 1$ at high frequencies when higher order modes start to play a bigger role. It is natural to wonder what is the exact frequency dependence for $1/T_1(\omega_0)$ at high frequencies when $r_i/r_f < 1$; an exhaustive study of this point is necessarily left for future investigations.

In the Supplementary Information we show that at $r_i/r_f = 0.375$ (for example), the percentage contribution from the first mode to $1/T_1(\omega_0)$ decreases as $\{71\%, 57\%, 39\%\}$ with increasing frequency $\omega_0 = \{0, 1/\tau_d, 2/\tau_d\} = \{0, 0.15, 0.30\}$, respectively, where τ_d is the BPP limit at $r_i/r_f = 1$ defined in Eq. (16). This highlights the importance of higher order modes ($k \geq 2$) in $1/T_1(\omega_0)$ with increasing ω_0 and decreasing r_i/r_f . Furthermore, for similar physical systems our formalism can determine how many modes are required to describe $1/T_1(\omega_0)$ within a specified accuracy, where an increasing number of modes ($k \geq 2$) will be required with increasing ω_0 and decreasing r_i/r_f .

D. Physical interpretation of modes

The physical interpretation of the molecular modes of NMR relaxation leads to the conclusion that they depend both on the dynamics and the structure of the system. The dynamic contribution can be understood as the effect of the diffusion constant D on the characteristic times τ_k , given by Eq. (25) for the case under study. This implies that low frictional (viscous) and highly diffusional systems will present shorter relaxation times. The structural effect on the molecular modes of relaxation arises from the individual contributions to the

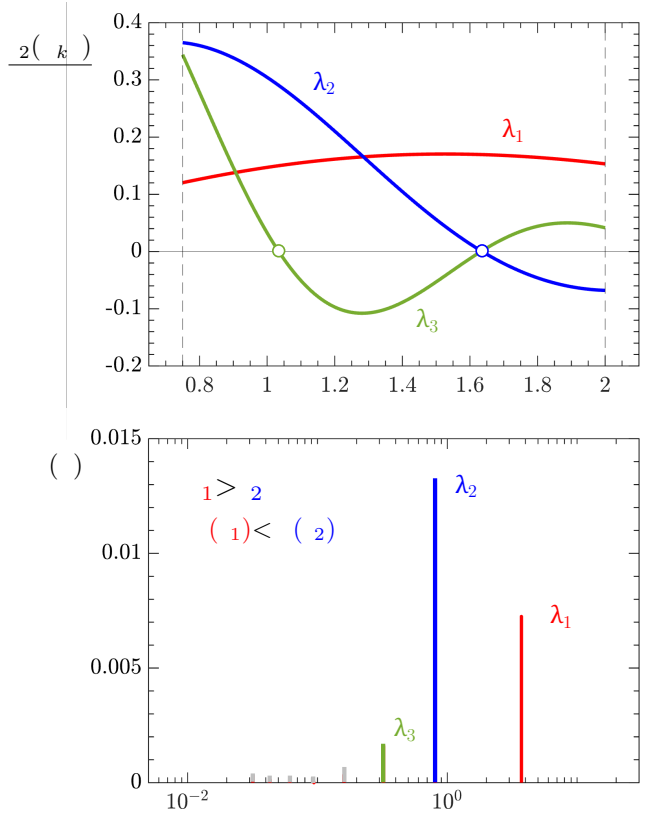
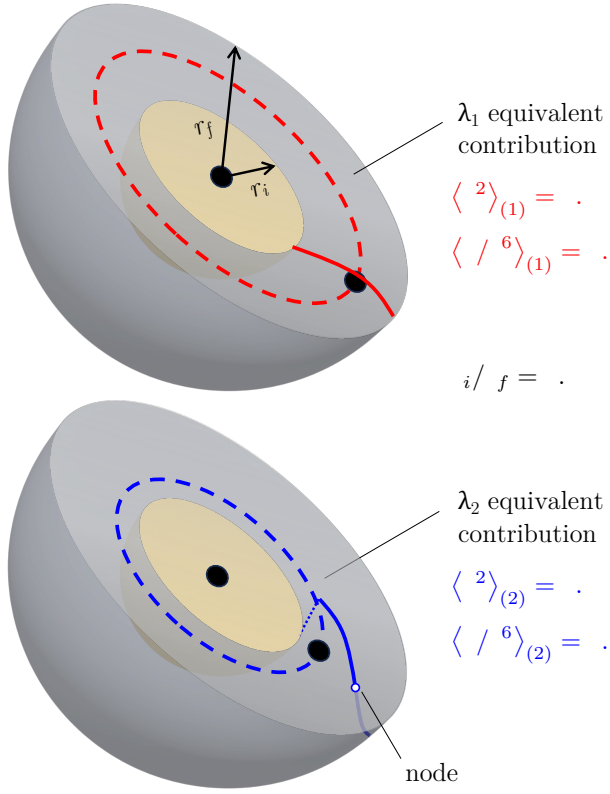


FIG. 10. Schematic representation of the molecular modes of NMR relaxation. The multi-modal (multi-exponential) decay arise from the different eigenvalues λ_k and their corresponding eigenfunctions. We observe the k^{th} contribution to the total radial probability distribution will present $k - 1$ nodes (zero probability points), and hence regions where the eigenfunction goes negative will present a depletion on the probability distribution. Each mode k has a corresponding $\langle r^2 \rangle_{(k)} \propto \tau_k$ and $\langle 1/r^6 \rangle_{(k)} \propto P(\tau_k)$ given by a weighted average through that mode's contribution to the (total) phase distribution function.

phase distribution function $\rho(\mathbf{r}, t)$ of the system between the limits r_i and r_f . This is analogous to how the quantum harmonic oscillator solution splits into different eigenstates, with discrete energies. In our case, the summation in Eq. (21) teaches us how the overall (physical) probability distribution partitions over the underlying subsets (states) defined by the eigenmodes, with discrete characteristic times. Figure 10 illustrates how the k^{th} mode, i.e. the k^{th} -eigenfunction, contributes to the probability distribution $\rho(\mathbf{r}, t)$. Notice that the mode corresponding to λ_k has $k - 1$ nodes in r , i.e., points where $j_2(\lambda_k r)/r = 0$ and thus $\rho(\mathbf{r}, t) = 0$. For each mode, the zones where the eigenfunction goes negative will usually involve a depletion of probability and conversely when the eigenfunction is positive. This implies that each k^{th} mode will contribute with a unique and inherent structural probability density in r , reminiscent of the idea of inherent structures in liquids⁶⁷.

Another way of interpreting these molecular modes of relaxation is by attributing an equivalent BPP-like rotational diffusion contribution to each of them. For any mode k , there will exist a weighted average leading to $\langle r^2 \rangle_{(k)}$ that is proportional to τ_k , and similarly a weighted average leading to $\langle 1/r^6 \rangle_{(k)}$ that is proportional to $P(\tau_k)$. The weight in these

averages is the mode's contribution to the total phase distribution function. By increasing the order of the mode k , $\langle r^2 \rangle_{(k)}$ will always decrease and get closer to the central dipole, signifying shorter characteristic times τ_k . On the other hand, $\langle 1/r^6 \rangle_{(k)}$ does not always increase with order of the mode k , and hence the corresponding amplitude $P(\tau_k)$ of each mode also depends on the radial spacing of the annulus. As implied in Eq. 41, the net effect of these two contributions on the relaxation rate $1/T_{1,2}$ from mode k alone is the product $P(\tau_k) \tau_k \propto \langle r^2 \rangle_{(k)} \langle 1/r^6 \rangle_{(k)}$.

Consider the first mode corresponding to λ_1 . This mode has no nodes in the radial direction. On average, this is equivalent to a rotational diffusion at $\langle r^2 \rangle_{(1)}$ close to the geometrical average $\langle r^2 \rangle$ between r_i and r_f , depending on how flat the corresponding probability density is in that spherical shell. Importantly, in the limit of $r_i/r_f \rightarrow 1$, the diffusion happens exactly at $\langle r^2 \rangle$, which is the BPP limit.

Next consider the second mode λ_2 . The corresponding eigenfunction has one node in the radial direction. Thus, the range of r where the density function is positive contributes positively to the average rotational diffusion of that mode, and conversely the negative part of the density function depletes

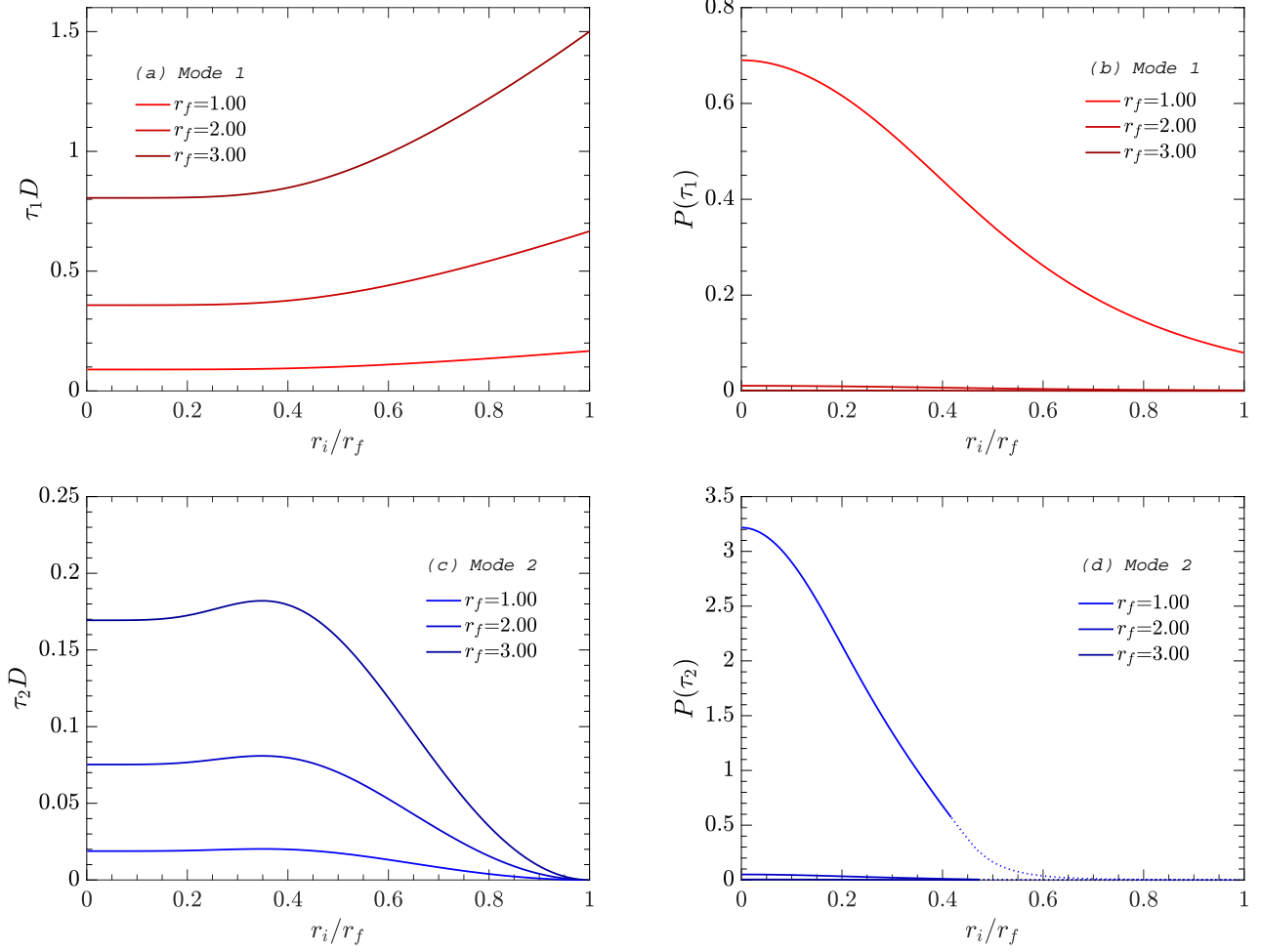


FIG. 11. Theoretical prediction of molecular modes characteristic times τ_k and corresponding amplitudes $P(\tau_k)$ for different r_f values, with $f = 10$ and $T = 1.0$. Plot (a) shows $\tau_1 D$ for the first molecular mode and plot (b) shows its corresponding amplitude $P(\tau_1)$ across r_i/r_f . Plot (c) shows $\tau_2 D$ for the second molecular mode and plot (d) shows its corresponding amplitude $P(\tau_2)$ across r_i/r_f .

the probability for its corresponding range of r . This gives rise to a unique averaged quantity $\langle r^2 \rangle_{(2)}$ (from the inherent structure of mode 2), which is associated with an equivalent rotational diffusion for the mode. In a similar fashion, one can interpret the contribution of the higher modes

We can gain further insights into above ideas. Since the magnitude of the NMR relaxation rate ($1/T_{1,2}$) is sensitive to the distance between the two dipoles, it proves helpful to investigate how the modes behave as we change the outer radius r_f . Physically, we expect that the larger the distance between the dipoles, the smaller the NMR relaxation rate. Figure 11 shows the characteristic times and corresponding amplitudes for the first two molecular modes across r_i/r_f , for different values of r_f .

Figures 11(a) and 11(c) show that the characteristic times τ_1 and τ_2 increase in magnitude as we increase r_f at constant diffusivity. This makes physical sense, given that a larger distance between the dipoles means that the second dipole will need to take a longer path to present a certain angular devia-

tion with respect to the central dipole and affect the angular terms that drive NMR relaxation. On the other hand, Figures 11(b) and 11(d) show that the amplitudes $P(\tau_1)$ and $P(\tau_2)$ decrease in magnitude as we increase r_f at constant diffusivity. This also agrees with the expected physical results, since the farther away the dipoles, the smaller the strength of NMR relaxation. In the limit that the two particles are infinitely distant (in this case, around $r_f \sim 3$ or greater), the amplitudes of such modes will decay to zero.

Interestingly, our results reveal a scaling behavior. For each characteristic time τ_k , the profiles for different r_i and r_f across r_i/r_f collapse to the same curve if we evaluate the normalized quantity $6D\tau_k/\langle r^2 \rangle$. Figures 12(a) and 12(c) illustrate that all curves match for the normalized τ_1 and τ_2 regardless of the actual spherical thickness for translational diffusion. Similarly, for each amplitude $P(\tau_k)$, the profiles for different r_i and r_f across r_i/r_f collapse to the same curve if we evaluate the normalized quantity $4\pi P(\tau_k)/\langle 1/r^6 \rangle$ (Figures 12(b) and 12(d)), regardless of the annulus thickness.

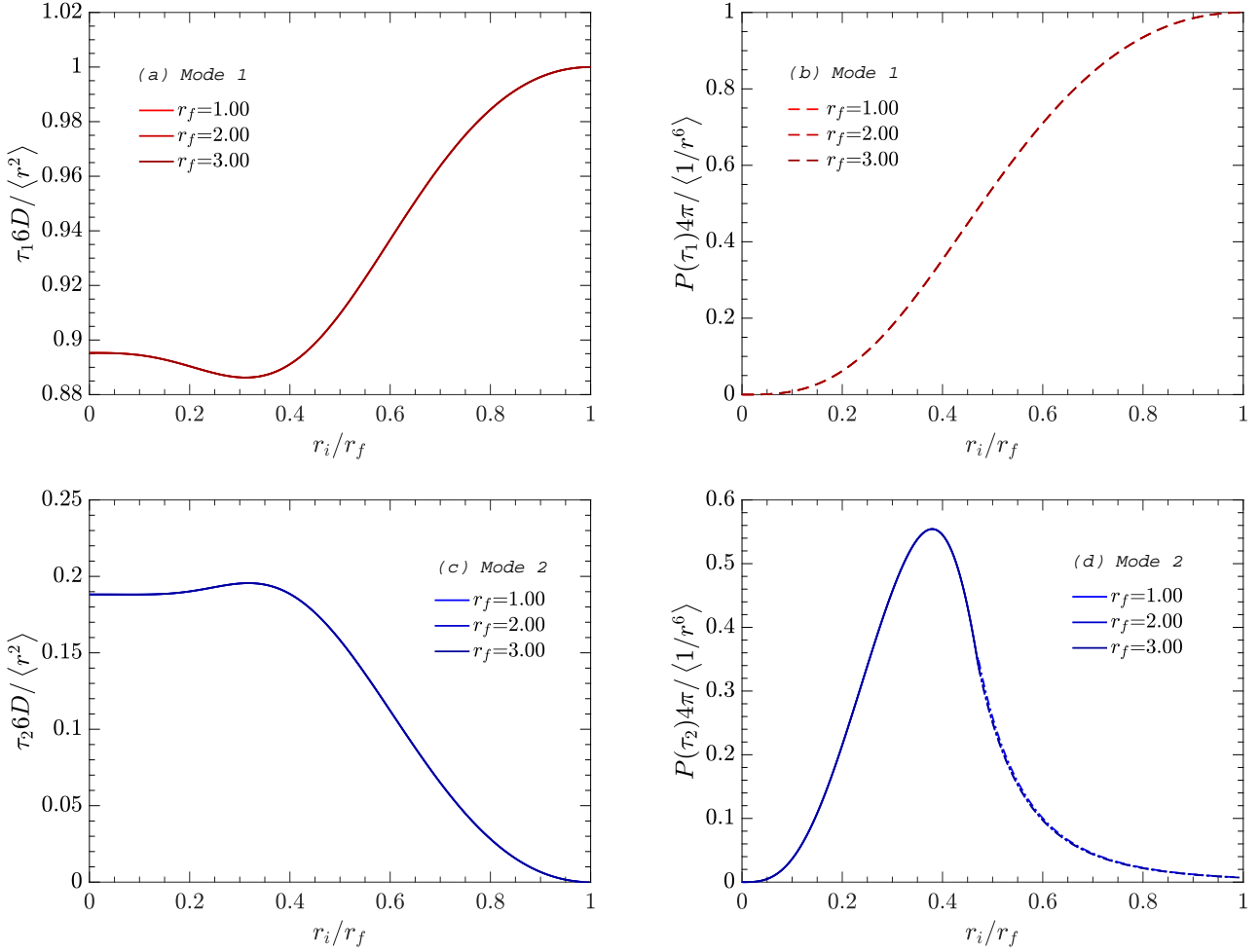


FIG. 12. Theoretical prediction of scaled molecular modes characteristic times $6D\tau_k/\langle r^2 \rangle$ and scaled amplitudes $4\pi P(\tau_k)/\langle 1/r^6 \rangle$ for different r_f values, with $f = 10$ and $T = 1.0$. Plot (a) shows $6D\tau_1/\langle r^2 \rangle$ for the first molecular mode and plot (b) shows its corresponding scaled amplitude $4\pi P(\tau_1)/\langle 1/r^6 \rangle$ across r_i/r_f . Plot (c) shows $6D\tau_2/\langle r^2 \rangle$ for the second molecular mode and plot (d) shows its corresponding scaled amplitude $4\pi P(\tau_2)/\langle 1/r^6 \rangle$ across r_i/r_f .

In the limit $r_i/r_f \rightarrow 1$ both the normalized characteristic time τ_1 and the amplitude $P(\tau_1)$ for the first mode converge to unity, while characteristic times and amplitudes for the higher modes converge to zero, as it should in the limit where BPP is valid (cf. Eqs. (16) and (17)). The fact that we are able to describe the entire profile of τ_k 's and $P(\tau_k)$'s over r_i/r_f is an advantage: one can use the normalized results to predict the characteristic time and amplitude for a mode for different spherical thicknesses, and for any absolute distance of interest between the dipoles.

Note that in the (non-physical) limit $r_i/r_f \rightarrow 0$, the amplitudes $P(\tau_k)$ remain finite for $k = \{1, 2\}$ (Figures 11(b,d)), while the normalized $4\pi P(\tau_k)/\langle 1/r^6 \rangle$ decay to zero for $k = \{1, 2\}$ due to the divergence $\langle 1/r^6 \rangle \rightarrow \infty$ (Figures 12(b,d)). In this limit, the amplitudes $P(\tau_k)$ grow with k , and $P(\tau_k) \rightarrow \infty$ diverge when $\tau_k \rightarrow 0$. Thus, in the non-physical limit of $r_i/r_f \rightarrow 0$, the contributions from modes $k = \{1, 2\}$ become increasingly negligible.

V. EXTENSIONS OF THE MODEL

We discuss some possible extensions of our formalism to other cases of physical interest. In the case of a system with m dipoles interacting with a central dipole c , the total equilibrium phase distribution function of the system is given by

$$\rho(\mathbf{r}, t) = \sum_{i=1}^m \rho_{c,i}(\mathbf{r}, t), \quad (43)$$

where $\rho_{c,i}(\mathbf{r}, t)$ is the probability function of finding dipole i around dipole c , for $i = 1, 2, 3, \dots, m$, and subject to the presence of all other dipoles in the system. If we again assume an isotropic system and that all the dipoles are non-interacting and constrained to lie in defined shells around the central dipole, we can get $\rho_{c,i}(\mathbf{r}, t)$ through the result derived in Eq. (21).

Consider, for example, two non-interacting dipoles around a central one. Figure 13 shows three different systems, hav-

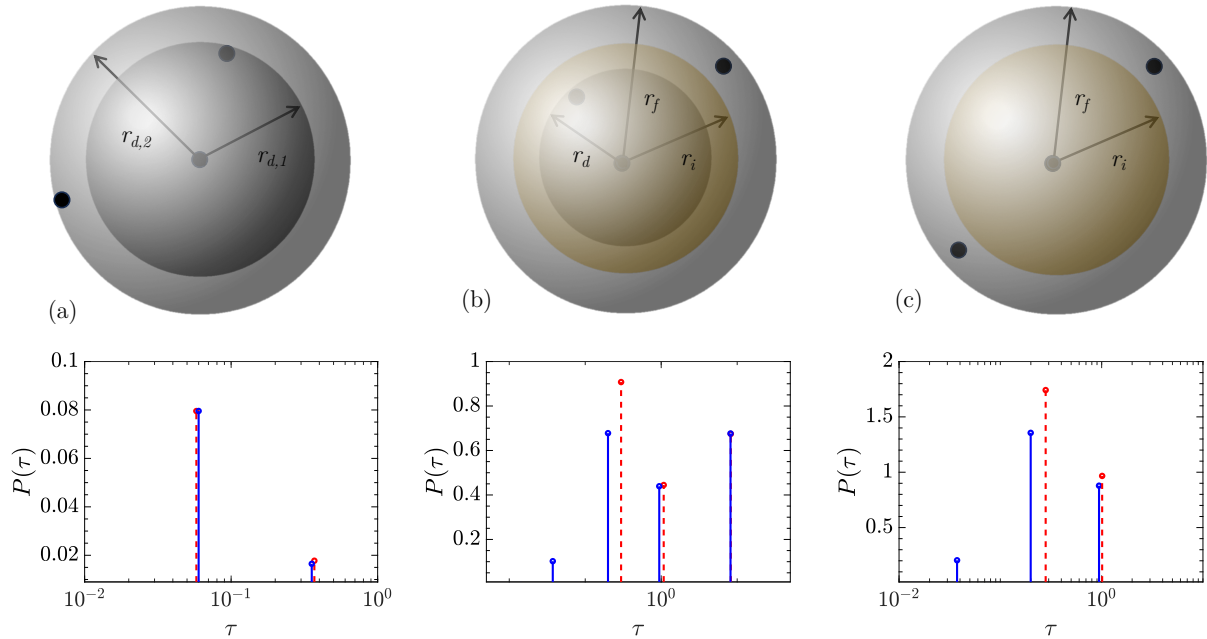


FIG. 13. Extended toy-cases of multiple non-interacting dipoles undergoing NMR relaxation with respect to a central dipole and their corresponding molecular modes distribution at $T = 1.00$. The solid lines represent the theoretical predictions, while the dashed lines represent the MD simulation results. Case (a) shows two dipoles around the central one at fixed distances $r_{d,1} = 1.00$ with $f_1 = 0.01$, and $r_{d,2} = 1.30$ and $f_2 = 0.10$. Case (b) shows one dipole at a fixed distance $r_d = 0.70$ with $f_1 = 0.01$, and another dipole at non-fixed distance diffusing between $r_i = 0.40$ and $r_f = 1.00$ with $f = 10$. Case (c) shows two dipoles at non-fixed distances diffusing between $r_i = 0.40$ and $r_f = 1.00$ with $f = 10$.

ing a central dipole and (a) two fixed dipoles around it, (b) one dipole at a fixed distance and another one diffusing on a thick spherical shell, and (c) two dipoles diffusing on a thick spherical shell. Observe that the NMR autocorrelation function for dipole pairs from MD simulations is a single averaged function that subsumes all the modes present in the system. The task for the Padé-Laplace inversion is to decode the underlying exponential decays. Hence, if the modes are above the frequency of sampling from the simulation and their amplitudes present a high signal-to-noise ratio, we find that the Padé-Laplace inversion will capture these modes. For this example, we find that the theory can also predict relatively well the multi-modal behavior.

Another possible extension is the inclusion of a potential of interaction $U(r)$ between the dipoles in Eq. (8), which would affect the corresponding $\rho(\mathbf{r}, t)$ and, ultimately, the molecular modes and the spin-spin and spin-lattice relaxation times. (Studies in this direction are underway and the results will be communicated later.) Finally, a natural extension of the model would be to investigate intra-molecular relaxation between dipoles in a chain (e.g., alkanes), by assuming that r_f is the maximum distance between the two dipoles when the chain is fully stretched, and r_i is the minimum distance between the dipoles when the chain is coiled at its maximum. In this case, however, relaxing boundary conditions would be needed instead of reflective ones, implying that SL-EVP for the calculation of the characteristic time will have a different mathematical form, and the definition of orthogonality of the eigenfunctions will change accordingly.

VI. CONCLUSION

We investigate the emergence of a multi-exponential NMR autocorrelation function for dipole pairs undergoing regular rotational and translational diffusion, and propose a theoretical framework to model such multi-exponential behavior, here coined as molecular modes of NMR relaxation. This multi-exponential behavior in the autocorrelation function leads to anomalous NMR relaxation dispersion compared to the traditional BPP model. A key feature is that there are no adjustable parameters in interpreting the NMR relaxation behavior. We examine the case of two non-interacting dipoles in a viscous and isotropic system, where distance between the dipoles can freely vary between defined lower and upper limits. Even this simple case leads to a multi-mode (multi-exponential) behavior, which our theory is able to capture. Such multi-exponential behavior of the NMR autocorrelation function essentially arises from a corresponding eigenvalue problem, that depends on the boundary conditions of the problem and the geometry of the systems. Molecular simulations associated with the Padé-Laplace inversion validate the theoretical predictions with good agreement.

Our investigations clarify the physical meaning of such molecular modes of NMR relaxation. The dynamics of the system directly impacts these characteristic times τ_k , which are inversely proportional to the diffusion constant D of the dipoles in the viscous fluid. However, structural effects also play a major role in these molecular modes, and we observe that different modes τ_k contribute to the solution with a corre-

sponding eigenfunction with $k - 1$ nodes in the radial direction (zero probability density). The first mode (largest characteristic time) has no nodes in the radial distribution, and then the averaged angular diffusion given by this mode happens on a sphere with radius close to the geometrical average $\langle r^2 \rangle$ over the full radial range. The higher-order modes present nodes in the radial distribution, and hence the averaged angular diffusion for such nodes happens in different equivalent radii.

A key result is that our theoretical formalism agrees with the traditional BPP theory in the limit where the distance between the two dipoles becomes constant ($r_i/r_f \rightarrow 1$). The model also agrees with the expected response in the limit where the two dipoles come close to each other ($r_i/r_f \rightarrow 0$), and it also supports the empirical observations that the temperature dependence of the modes' characteristic times τ_k follows an Arrhenius-like model for high temperatures. For the cases studied in this work, the characteristic times of the molecular modes τ_k and their corresponding amplitudes $P(\tau_k)$ can be scaled by $6D\tau_k/\langle r^2 \rangle$ and $4\pi P(\tau_k)/\langle 1/r^6 \rangle$, respectively. This allows us to predict the molecular modes and the corresponding amplitudes for any r_i and r_f combination between the dipoles undergoing relaxation.

We have also presented the NMR dispersion for $1/T_1(\omega_0)$ for the case of like-spins, showing that the importance of higher order modes (and hence, the deviation from the BPP model) increases with increasing ω_0 and decreasing r_i/r_f . Finally, we discussed some extensions of our formalism and future work to cover more cases of interest, like the case with potential of interaction or the intramolecular relaxation of dipole pairs in a molecular chain. Being able to model and understand the individual modes that lead to NMR dipole-dipole relaxation can provide crucial physical insights into phenomena on the molecular level.

ACKNOWLEDGEMENTS

The authors thank Arjun Valya Parambathu for the insightful discussions. We also thank the Ken Kennedy Institute, the Rice University Creative Ventures Fund (Faculty Initiatives Fund), and the Robert A. Welch Foundation for the financial support. We gratefully acknowledge the National Energy Research Scientific Computing Center, which is supported by the Office of Science of the U.S. Department of Energy (No. DE-AC02-05CH11231) and the Texas Advanced Computing Center (TACC) at The University of Texas at Austin for high-performance computer time and support. Research at Oak Ridge National Laboratory is supported under contract DE-AC05-00OR22725 from the U.S. Department of Energy to UT-Battelle, LLC. This research used resources of National Energy Research Scientific Computing Center, which is supported by the Office of Science of the U.S. Department of Energy under Contract # DE-AC02-05CH11231.

SUPPLEMENTARY INFORMATION

The Supplementary Information provides the detailed analytical solution of the NMR dipole-dipole autocorrelation function for the cases of fixed and non-fixed distance between the dipoles, as well as the comparison between our theoretical predictions and MD simulations raw data for the modes' amplitudes and characteristic times for all studied cases. We have also included a comparison of the NMR dipole-dipole autocorrelation obtained using MD simulations and the corresponding reconstructed signal using the Padé-Laplace method. Moreover, we provide an analysis of the accuracy of the numerical approximations made to compute integrals using the regular Euclidean definition of inner-product. Finally, we provide the theoretical breakdown contribution from different molecular modes to NMR relaxation dispersion.

DATA AVAILABILITY

The data that support the findings of this study are available from the corresponding authors upon reasonable request.

REFERENCES

- B. J. Berne and R. Pecora, *Dynamic light scattering with applications to chemistry, biology, and physics*, 1st ed., Vol. 1 (John Wiley & Sons, Inc., 2000).
- E. D. Becker, *High resolution NMR: Theory and chemical applications*, 3rd ed. (Academic Press, 2000).
- W. S. Price, *NMR studies of translational motion: Principles and applications*, 1st ed. (Cambridge University Press, 2009).
- W. B. Moniz, W. A. Steele, and J. A. Dixon, "Nuclear spin relaxation in liquids. Spheroidal molecules," *The Journal of Chemical Physics* **38**, 2418–2426 (1963).
- P. M. Singer, D. Asthagiri, W. G. Chapman, and G. J. Hirasaki, "Molecular dynamics simulations of NMR relaxation and diffusion of bulk hydrocarbons and water," *Journal of Magnetic Resonance* **277**, 15–24 (2017).
- P. M. Singer, D. Asthagiri, Z. Chen, A. V. Parambathu, G. J. Hirasaki, and W. G. Chapman, "Role of internal motions and molecular geometry on the NMR relaxation of hydrocarbons," *Journal of Chemical Physics* **148**, 1–10 (2018).
- P. M. Singer, D. Asthagiri, W. G. Chapman, and G. J. Hirasaki, "NMR spin-rotation relaxation and diffusion of methane," *Journal of Chemical Physics* **148**, 204504 (2018).
- D. Asthagiri, W. G. Chapman, G. J. Hirasaki, and P. M. Singer, "NMR ^1H - ^1H dipole relaxation in fluids: Relaxation of individual ^1H - ^1H pairs versus relaxation of molecular modes," *Journal of Physical Chemistry B* **124**, 10802–10810 (2020).
- P. M. Singer, A. Valiya Parambathu, X. Wang, D. Asthagiri, W. G. Chapman, G. J. Hirasaki, and M. Fleury, "Elucidating the ^1H NMR relaxation mechanism in polydisperse polymers and bitumen using measurements, MD simulations, and models," *Journal of Physical Chemistry B* **124**, 4222–4233 (2020).
- A. Valiya Parambathu, P. M. Singer, G. J. Hirasaki, W. G. Chapman, and D. Asthagiri, "Critical role of confinement in the NMR surface relaxation and diffusion of *n*-heptane in a polymer matrix revealed by MD simulations," *Journal of Physical Chemistry B* **124**, 3801–3810 (2020).
- A. Valiya Parambathu, W. G. Chapman, G. J. Hirasaki, D. Asthagiri, and P. M. Singer, "Effect of nanoconfinement on NMR relaxation of heptane in kerogen from molecular simulations and measurements," *Journal of Physical Chemistry Letters* **14** (4), 1059–1065 (2023).

- ¹²P. M. Singer, A. V. Parambathu, T. J. P. D. Santos, Y. Liu, L. B. Alemany, G. J. Hirasaki, W. G. Chapman, and D. Asthagiri, "Predicting ^1H NMR relaxation in Gd^{3+} -aqua using molecular dynamics simulations," *Physical Chemistry and Chemical Physics* **23**, 20974–20984 (2021).
- ¹³T. J. Pinheiro dos Santos, A. V. Parambathu, C. C. Fraenza, C. Walsh, S. G. Greenbaum, W. G. Chapman, D. Asthagiri, and P. M. Singer, "Thermal and concentration effects on ^1H NMR relaxation of Gd^{3+} -aqua using MD simulations and measurements," *Physical Chemistry Chemical Physics* **24**, 27964–27975 (2022).
- ¹⁴R. Brüschweiler, B. Roux, M. Blackledge, C. Griesinger, M. Karplus, and R. R. Ernst, "Influence of rapid intramolecular motion on NMR cross-relaxation rates. A molecular dynamics study of antamanide in solution," *Journal of the American Chemical Society* **114**, 2289–2302 (1992).
- ¹⁵M. Lindgren, A. Laaksonen, and P.-O. Westlund, "A theoretical spin relaxation and molecular dynamics simulation study of the $\text{Gd}(\text{H}_2\text{O})_9^{3+}$ complex," *Physical Chemistry and Chemical Physics* **11**, 10368–10376 (2009).
- ¹⁶D. A. Faux, S. H. P. Cachia, P. J. McDonald, J. S. Bhatt, N. C. Howlett, and S. V. Churakov, "Model for the interpretation of nuclear magnetic resonance relaxometry of hydrated porous silicate materials," *Physical Review E* **91**, 032311 (2015).
- ¹⁷M. Becher, T. Wohlfromm, E. A. Rössler, and M. Vogel, "Molecular dynamics simulations vs field-cycling NMR relaxometry: Structural relaxation mechanisms in the glass-former glycerol revisited," *Journal of Chemical Physics* **154**, 124503 (2021).
- ¹⁸W. M. Madhavi, S. Weerasinghe, and K. I. Momot, "Reorientational dynamics of molecules in liquid methane: A molecular dynamics simulation study," *Journal of Molecular Liquids* **324**, 114727 (2021).
- ¹⁹J. B. B. Beckmann, D. Rauber, F. Philippi, K. Goloviznina, J. A. Ward-Williams, A. J. Sederman, M. D. Mantle, A. Pádua, C. W. M. Kay, T. Welton, and L. F. Gladden, "Molecular dynamics of ionic liquids from fast-field cycling NMR and molecular dynamics simulations," *Journal of Physical Chemistry B* **126**, 7143–7158 (2022).
- ²⁰I. Rybin, I. Shikhov, and C. H. Arns, "Lattice Boltzmann framework for accurate NMR simulation in porous media," *Physical Review E* **105**, 055304 (2022).
- ²¹Y. Wang, J. I. Amaro-Estrada, and C. Torres-Verdín, "Molecular insights into nuclear-magnetic-resonance properties of NaCl solution confined within calcite nanopores," *Colloids and Surfaces A* **673**, 131721 (2023).
- ²²A. Phillips and J. Autschbach, "Unified description of proton NMR relaxation in water, acetonitrile, and methane from molecular dynamics simulations in the liquid, supercritical, and gas phases," *Journal of Physical Chemistry B* **127** (5), 1167–1177 (2023).
- ²³J. I. Amaro-Estrada, Y. Wang, and C. Torres-Verdín, "Structural and nuclear magnetic resonance relaxation properties of shale condensate within organic nanopores via molecular dynamics simulations," *Energy & Fuels* **37** (14), 10318–10328 (2023).
- ²⁴S. Gravelle, D. Beyer, M. Brito, A. Schlaich, and C. Holm, "Assessing the validity of NMR relaxation rates obtained from coarse-grained simulations of PEG–water mixtures," *Journal of Physical Chemistry B* **127** (15), 5601–5608 (2023).
- ²⁵Y. Wang, J. I. Amaro-Estrada, and C. Torres-Verdín, "Role of paramagnetic impurities and surface roughness on NMR relaxation times: Insights from molecular dynamics simulations," *Journal of Physical Chemistry C* (2023), 10.1021/acs.jpcc.3c02580.
- ²⁶Y. Wang, J. I. Amaro-Estrada, and C. Torres-Verdín, "Quantifying magnetic resonance effects due to solid-fluid interactions on confined water within quartz-lined nanopores via molecular dynamics simulations," *Journal of Physical Chemistry C* **127**, 4283–4294 (2023).
- ²⁷N. Bloembergen, E. M. Purcell, and R. V. Pound, "Relaxation effects in nuclear magnetic resonance absorption," *Physical Review* **73**, 679–712 (1948).
- ²⁸D. E. Woessner, "Nuclear magnetic dipole-dipole relaxation in molecules with internal motion," *The Journal of Chemical Physics* **42**, 1855–1859 (1965).
- ²⁹W. A. Steele, "Molecular reorientation in liquids. I. Distribution functions and friction constants," *The Journal of Chemical Physics* **38**, 2404–2410 (1963).
- ³⁰K. R. Brownstein and C. E. Tarr, "Importance of classical diffusion in NMR studies of water in biological cells," *Physical Review A* **19**, 2446–2453 (1979).
- ³¹G. Lipari and A. Szabo, "Model-free approach to the interpretation of nuclear magnetic resonance relaxation in macromolecules. 1. Theory and range of validity," (1982).
- ³²M. C. Martínez and J. G. de la Torre, "Brownian dynamics simulation of restricted rotational diffusion," *Biophysical Journal* **52**, 303–310 (1987).
- ³³G. Williams and D. C. Watts, "Non-symmetrical dielectric relaxation behaviour arising from a simple empirical decay function," *Trans. Faraday Soc.* **66**, 80–85 (1970).
- ³⁴D. W. Davidson and R. H. Cole, "Dielectric relaxation in glycerol, propylene glycol, and *n*-propanol," *Journal of Chemical Physics* **19**, 1484 (1951).
- ³⁵G. Lipari and A. Szabo, "Model-Free approach to the interpretation of nuclear magnetic resonance relaxation in macromolecules. 1. Theory and range of validity," *Journal of the American Chemical Society* **104**, 4546–4559 (1982).
- ³⁶I. Solomon, "Relaxation processes in a system of two spins," *Physical Review* **99**, 559–565 (1955).
- ³⁷N. Bloembergen and L. O. Morgan, "Proton relaxation times in paramagnetic solutions. Effects of electron spin relaxation," *The Journal of Chemical Physics* **34**, 842–850 (1961).
- ³⁸J. Wahsner, E. M. Gale, A. Rodríguez-Rodríguez, and P. Caravan, "Chemistry of MRI contrast agents: current challenges and new frontiers," *Chemical Reviews* **119**, 957–1057 (2019).
- ³⁹H. C. Torrey, "Nuclear spin relaxation by translational diffusion," *Physical Review* **92** (1953).
- ⁴⁰L. P. Hwang and J. H. Freed, "Dynamic effects of pair correlation functions on spin relaxation by translational diffusion in liquids," *The Journal of Chemical Physics* **63**, 4017–4025 (1975).
- ⁴¹D. E. Woessner, "Nuclear spin relaxation in ellipsoids undergoing rotational brownian motion," *The Journal of Chemical Physics* **37**, 647–654 (1962).
- ⁴²D. E. Woessner, "Spin relaxation processes in a two-proton system undergoing anisotropic reorientation," *The Journal of Chemical Physics* **36**, 1–4 (1962).
- ⁴³D. E. Woessner and B. S. Snowden, "Magnetic relaxation under hindered rotation in fluids," *Advances in Molecular Relaxation Processes* **3**, 181–197 (1972).
- ⁴⁴W. A. Steele, "Molecular reorientation in liquids. II. Angular autocorrelation functions," *The Journal of Chemical Physics* **38**, 2411–2418 (1963).
- ⁴⁵B. Ghadirian, A. M. Torres, N. N. Yadav, and W. S. Price, "Restricted diffusion in annular geometrical pores," *Journal of Chemical Physics* **138** (2013), 10.1063/1.4793525.
- ⁴⁶T. Zavada, N. Sü. R. Kimmich, and T. F. Nonnenmacher, "Propagator representation of anomalous diffusion: The orientational structure factor formalism in NMR," *Physical Review E* **60**, 1292–1298 (1999).
- ⁴⁷C. H. Neuman, "Spin echo of spins diffusing in a bounded medium," *The Journal of Chemical Physics* , 4508–4511 (1974).
- ⁴⁸D. S. Grebenkov, "Analytical solution for restricted diffusion in circular and spherical layers under inhomogeneous magnetic fields," *Journal of Chemical Physics* **128** (2008), 10.1063/1.2841367.
- ⁴⁹J. McConnell, *The theory of nuclear magnetic relaxation in liquids*, 1st ed. (Cambridge University Press, 2009).
- ⁵⁰C. H. Ziener, T. Kampf, and F. T. Kurz, "Diffusion propagators for hindered diffusion in open geometries," *Concepts in magnetic resonance part A: Bridging education and research* **44**, 150–159 (2015).
- ⁵¹D. Caldas, J. Chahine, and E. D. Filho, "The Fokker-Planck equation for a bistable potential," *Physica A: Statistical Mechanics and its Applications* **412**, 92–100 (2014).
- ⁵²J. Piasecki, "Centenary of marian Smoluchowski's theory of Brownian motion," *Acta Physica Polonica B* **38**, 1623–1629 (2007).
- ⁵³P. Bernatowicz, J. Kowalewski, and S. Szymanski, "Nuclear-spin relaxation in nonrigid molecules: Discrete multisite local dynamics combined with anisotropic molecular reorientation," *Journal of Chemical Physics* **124** (2006), 10.1063/1.2149858.
- ⁵⁴J. Mitchell, A. Souza, E. Fordham, and A. Boyd, "A finite element approach to forward modeling of nuclear magnetic resonance measurements in coupled pore systems," *Journal of Chemical Physics* **150**, 154708 (2019).
- ⁵⁵P. Yan, F. Marica, J. Guo, and B. J. Balcom, "Direct measurement of pore size and surface relaxivity with magnetic resonance at variable temperature," *Physical Review Applied* **20**, 014009 (2023).

- ⁵⁶G. Arfken, *Mathematical methods for physicists*, 3rd ed. (Academic Press, 1985).
- ⁵⁷W. T. Reid, *Sturmian theory for ordinary differential equations*, 1st ed. (Spring-Verlag, 1980).
- ⁵⁸F. N. Hildebrand, *Methods of applied mathematics*, 1st ed. (Prentice-Hall, 1952).
- ⁵⁹S. Plimpton, "Fast parallel algorithms for short-range molecular dynamics," *Journal of Computational Physics* **117**, 1–19 (1995).
- ⁶⁰J. D. Weeks, D. Chandler, and H. C. Andersen, "Role of repulsive forces in determining the equilibrium structure of simple liquids," *The Journal of Chemical Physics* **54**, 5237–5247 (1971).
- ⁶¹E. H. Hellen, "Padé-Laplace analysis of signal averaged voltage decays obtained from a simple circuit," *American Journal of Physics* **73**, 871–875 (2005).
- ⁶²E. Yeramian and P. Claverie, "Analysis of multiexponential functions without a hypothesis as to the number of components," *Letters to Nature* **326**, 169–174 (1987).
- ⁶³T. M. Inc., "Matlab version: 9.13.0 (r2022b)," (2022).
- ⁶⁴A. G. Gad, "Particle swarm optimization algorithm and its applications: A systematic review," *Archives of Computational Methods in Engineering* **29**, 2531–2561 (2022).
- ⁶⁵D. T. Lin and C. K. Chen, "A molecular dynamics simulation of tip4p and lennard-jones water in nanochannel," *Acta Mechanica* **173**, 181–194 (2004).
- ⁶⁶L. C. Johnson and F. R. Phelan, "Comparison of friction parametrization from dynamics and material properties for a coarse-grained polymer melt," *Journal of Physical Chemistry B* (2023), 10.1021/acs.jpcc.3c03273.
- ⁶⁷F. H. Stillinger and T. A. Weber, "Inherent structure in water," *J. Phys. Chem* **87**, 2833–2840 (1983).

Supplementary Information: Theory and modeling of molecular modes in the NMR relaxation of fluids

Thiago J. Pinheiro dos Santos,¹ Betul Orcan-Ekmekci,² Walter G. Chapman,¹ Philip M. Singer,¹ and Dilipkumar N. Asthagiri³

¹*Department of Chemical and Biomolecular Engineering, Rice University, Houston, Texas 77005, USA.*

²*Department of Mathematics, Rice University, Houston, Texas 77005, USA.*

³*Oak Ridge National Laboratory, Oak Ridge, Tennessee 37830, USA.*

(*Electronic mail: asthagiridn@ornl.gov)

(*Electronic mail: ps41@rice.edu)

(Dated: 9 January 2024)

Notice: This manuscript has been authored by UT-Battelle, LLC, under contract DE-AC05-00OR22725 with the US Department of Energy (DOE). The US government retains and the publisher, by accepting the article for publication, acknowledges that the US government retains a nonexclusive, paid-up, irrevocable, worldwide license to publish or reproduce the published form of this manuscript, or allow others to do so, for US government purposes. DOE will provide public access to these results of federally sponsored research in accordance with the DOE Public Access Plan (<http://energy.gov/downloads/doe-public-access-plan>).

CONTENTS

A. Fixed distance and non-interacting dipoles	2
B. Non-fixed distance and non-interacting dipoles	5
C. Padé-Laplace inversion of $G(t)$	10
D. Numerical approximations for integral computations	13
E. Molecular modes via theory and MD simulations	16
F. Mode contributions to relaxation dispersion	18
References	21

A. Fixed distance and non-interacting dipoles

Let us consider the case where two, non-interacting dipoles are at fixed distance r_d . For convenience, we fix one of the dipoles at the center of coordinates, and solve for the probability density of the second dipole around the central one. In spherical coordinates, we have $\mathbf{r}_d = \{r_d, \theta, \phi\}$ and $U(\mathbf{r}_d) = 0$. Hence, Eq. (8) can be written as

$$\frac{\partial}{\partial t} \rho(\mathbf{r}_d, t) = D \nabla_r^2 \rho(\mathbf{r}_d, t). \quad (\text{S1})$$

where the Laplacian operator at constant $r = r_d$ is given by

$$\nabla_r^2 = -\frac{\hat{I}^2}{r_d^2} = \frac{1}{r_d^2 \sin \theta} \frac{\partial}{\partial \theta} \left(\sin \theta \frac{\partial}{\partial \theta} \right) + \frac{1}{r_d^2 \sin^2 \theta} \frac{\partial^2}{\partial \phi^2}, \quad (\text{S2})$$

where \hat{I}^2 is the angular momentum operator from quantum mechanics. This problem should be solved observing periodic boundary condition for the angular terms, i.e., $\rho(r_d, \theta, \phi, t) = \rho(r_d, \theta + \pi, \phi, t)$ and $\rho(r_d, \theta, \phi, t) = \rho(r_d, \theta, \phi + 2\pi, t)$.

Assuming separation of variables, the solution $\rho(\mathbf{r}_d, t)$ can be written as

$$\rho(\mathbf{r}_d, t) = T(t) \Phi(\theta, \phi) \quad (\text{S3})$$

where $T(t)$ is the part of the solution that depends only on time, and $\Phi(\theta, \phi)$ contains the angular dependence of the solution. Substituting Eq. (S3) into Eq. (S1), we find that

$$\frac{r_d^2}{DT(t)} \frac{\partial}{\partial t} T(t) = \frac{1}{\Phi(\theta, \phi)} \left(\frac{1}{\sin \theta} \frac{\partial}{\partial \theta} \left(\sin \theta \frac{\partial}{\partial \theta} \right) \Phi(\theta, \phi) + \frac{1}{\sin^2 \theta} \frac{\partial^2}{\partial \phi^2} Y(\theta, \phi) \right) \Phi(\theta, \phi) = -n(n+1), \quad (\text{S4})$$

in which the first term of the equality only depends on time, the second one only depends on the angular components, and then both should be equal to a constant $-n(n+1)$ chosen for convenience.

Therefore, the time-dependent part will be given by

$$\begin{aligned} \frac{1}{T(t)} \frac{\partial}{\partial t} T(t) &= -\frac{n(n+1)D}{r_d^2} \\ T(t) &= C_1 \exp \left(-\frac{n(n+1)D}{r_d^2} t \right) \end{aligned} \quad (\text{S5})$$

where C_1 is a constant of integration. On the other hand, the angular-dependent part will be given by

$$\begin{aligned} \left(\frac{1}{\sin \theta} \frac{\partial}{\partial \theta} \left(\sin \theta \frac{\partial}{\partial \theta} \right) Y(\theta, \phi) + \frac{1}{\sin^2 \theta} \frac{\partial^2}{\partial \phi^2} Y(\theta, \phi) \right) Y(\theta, \phi) &= -n(n+1)Y(\theta, \phi) \\ \hat{I}^2 \Phi(\theta, \phi) &= n(n+1)\Phi(\theta, \phi). \end{aligned} \quad (\text{S6})$$

NMR modes

At this point, it is important to recognize that the eigenfunctions and eigenvalues of the angular momentum operator follow

$$\hat{L}^2 Y_n^m(\theta, \phi) = n(n+1) Y_n^m(\theta, \phi). \quad (\text{S7})$$

where $Y_n^m(\theta, \phi)$ are the spherical harmonic functions associated with the corresponding Legendre polynomials of order n and m , i.e., $P_n^m(x)$. Hence, the angular-dependent solution $\Phi(\theta, \phi)$ is given by the linear combination of spherical harmonic functions, i.e.,

$$\Phi(\theta, \phi) = \sum_{n=0}^{\infty} \sum_{m=-n}^n C_{n,m} Y_n^m(\theta, \phi). \quad (\text{S8})$$

Finally, the solution for $\rho(r_d, \theta, \phi, t)$ is given by

$$\rho(\mathbf{r}_d, t) = \sum_{n=0}^{\infty} \sum_{m=-n}^n A_{n,m} Y_n^m(\theta, \phi) \exp\left(-\frac{n(n+1)D}{r_d^2} t\right) \quad (\text{S9})$$

where the coefficients $A_{n,m}$ depend on the initial condition $\rho(\mathbf{r}_d, 0)$ as

$$A_{n,m} = \frac{\int_0^{2\pi} \int_0^\pi \rho(\mathbf{r}_d, 0) Y_n^m(\theta, \phi) \sin \theta d\theta d\phi}{\int_0^{2\pi} \int_0^\pi |Y_n^m(\theta, \phi)|^2 \sin \theta d\theta d\phi}. \quad (\text{S10})$$

The initial distribution of the system is given by the delta functions at an initial configuration $\{r_d, \theta_0, \phi_0\}$, which is proportional to the spherical harmonic closure relationship¹, i.e.,

$$\begin{aligned} \rho(\mathbf{r}_d, 0) &= \frac{\delta(\theta - \theta_0) \delta(\phi - \phi_0)}{\sin \theta} p(\mathbf{r}_d, 0) \\ &= p(\mathbf{r}_d, 0) \sum_{n=0}^{\infty} \sum_{m=-n}^n Y_n^{m*}(\theta, \phi) Y_n^m(\theta_0, \phi_0) \end{aligned} \quad (\text{S11})$$

where the probability $p(\mathbf{r}_d, 0)$ of having the initial condition configuration at equilibrium is given by

$$\begin{aligned} p(\mathbf{r}_d, 0) &= \frac{p(\theta_0) p(\phi_0)}{\sin \theta_0} \\ &= \frac{1}{\sin \theta_0} \frac{\sin \theta_0}{\int_0^\pi \sin \theta d\theta} \frac{1}{\int_0^{2\pi} d\phi} \\ &= \frac{1}{4\pi}, \end{aligned} \quad (\text{S12})$$

such that

$$\rho(\mathbf{r}_d, 0) = \frac{1}{4\pi} \sum_{n=0}^{\infty} \sum_{m=-n}^n Y_n^{m*}(\theta, \phi) Y_n^m(\theta_0, \phi_0). \quad (\text{S13})$$

NMR modes

In NMR relaxation, we are only interested in the second moment ($n = 2$), and we will also assume that the system is isotropic ($m = 0$). Thus, the general solution to $\rho(\mathbf{r}_d, t)$ simplifies to

$$\rho(\mathbf{r}_d, t) = A_{2,0} Y_2^m(\theta, \phi) \exp\left(-\frac{6D}{r_d^2} t\right), \quad (\text{S14})$$

with the corresponding initial condition

$$\rho(\mathbf{r}_d, 0) = \frac{1}{4\pi} Y_2^{0*}(\theta, \phi) Y_2^0(\theta_0, \phi_0). \quad (\text{S15})$$

Thus, the coefficient $A_{2,0}$ is given by

$$\begin{aligned} A_{2,0} &= \frac{1}{4\pi} \frac{\int_0^{2\pi} \int_0^\pi Y_2^{0*}(\theta, \phi) Y_2^0(\theta_0, \phi_0) Y_2^0(\theta, \phi) \sin \theta d\theta d\phi}{\int_0^{2\pi} \int_0^\pi |Y_2^0(\theta, \phi)|^2 \sin \theta d\theta d\phi} \\ &= \frac{1}{4\pi} Y_2^0(\theta_0, \phi_0), \end{aligned} \quad (\text{S16})$$

in which we consider the orthogonality of spherical harmonics².

The final solution to the time-dependent equilibrium distribution probability between the two dipoles undergoing NMR relaxation at constant distance is given by

$$\rho(\mathbf{r}_d, t) = \frac{1}{4\pi} Y_2^{0*}(\theta, \phi) Y_2^0(\theta_0, \phi_0) \exp\left(-\frac{6Dt}{r_d^2}\right). \quad (\text{S17})$$

Using this result in Eq. (5) without integrating over the constant r_d , we find that

$$\begin{aligned} G(t) &= \frac{4\pi}{5} \left(\frac{\mu_0}{4\pi}\right)^2 \hbar^2 \gamma_I^2 \gamma_S^2 S(S+1) \frac{1}{4\pi} \frac{1}{r_d^6} \exp\left(-\frac{6Dt}{r_d^2}\right) \\ &\quad \int_0^{2\pi} \int_0^\pi Y_2^0(\theta_0, \phi_0) Y_2^0(\theta, \phi) \sin \theta d\theta_0 d\phi_0 \int_0^{2\pi} \int_0^\pi Y_2^{0*}(\theta, \phi) Y_2^0(\theta, \phi) \sin \theta d\theta d\phi, \end{aligned} \quad (\text{S18})$$

and by the orthogonality of the spherical harmonics, we obtain that

$$G(t) = \frac{4\pi}{5} \left(\frac{\mu_0}{4\pi}\right)^2 \hbar^2 \gamma_I^2 \gamma_S^2 S(S+1) \frac{1}{4\pi r_d^6} \exp\left(-\frac{6Dt}{r_d^2}\right). \quad (\text{S19})$$

This result is simply the mono-exponential decay from the traditional BPP theory that has been derived in different ways by others^{3,4}.

B. Non-fixed distance and non-interacting dipoles

Let us next consider the case where the two, non-interacting dipoles are not at fixed distance. Again, we fix one of the dipoles at the center of coordinates for convenience. If we adopt spherical coordinates to solve the problem, we have that $\mathbf{r} = \{r, \theta, \phi\}$, $U(\mathbf{r}) = 0$, and Eq. (8) becomes

$$\frac{\partial}{\partial t} \rho(\mathbf{r}, t) = D \nabla^2 \rho(\mathbf{r}, t), \quad (\text{S20})$$

where the full Laplacian operator is given by

$$\nabla^2 = -\frac{\hat{L}^2}{r^2} = \frac{1}{r^2} \frac{\partial}{\partial r} \left(r^2 \frac{\partial}{\partial r} \right) + \frac{1}{r^2 \sin \theta} \frac{\partial}{\partial \theta} \left(\sin \theta \frac{\partial}{\partial \theta} \right) + \frac{1}{r^2 \sin^2 \theta} \frac{\partial^2}{\partial \phi^2}. \quad (\text{S21})$$

Again, this problem should be solved observing periodic boundary condition for the angular terms as in $\rho(r, \theta, \phi, t) = \rho(r, \theta + \pi, \phi, t)$ and $\rho(r, \theta, \phi, t) = \rho(r, \theta, \phi + 2\pi, t)$. We employed Neumann boundary conditions for the radial term (reflecting boundary conditions), given by

$$\begin{aligned} \left. \frac{\partial \rho(r, \theta, \phi, t)}{\partial r} \right|_{r=r_i} &= 0, \\ \left. \frac{\partial \rho(r, \theta, \phi, t)}{\partial r} \right|_{r=r_f} &= 0. \end{aligned} \quad (\text{S22})$$

Assuming separation of variables, the solution $\rho(\mathbf{r}, t)$ can be written as

$$\rho(\mathbf{r}, t) = T(t)R(r)\Phi(\theta, \phi), \quad (\text{S23})$$

where $T(t)$ is the part of the solution that depends only on time, $R(r)$ is the radial dependent solution, and $\Phi(\theta, \phi)$ contains the angular dependency of the solution. Hence, by substituting Eq. (S23) into Eq. (S20), we find that

$$\begin{aligned} \frac{1}{DT(t)} \frac{\partial}{\partial t} T(t) &= \frac{1}{r^2 R(r)} \frac{\partial}{\partial r} \left(r^2 \frac{\partial}{\partial r} \right) R(r) + \frac{1}{\Phi(\theta, \phi)} \frac{1}{r^2 \sin \theta} \frac{\partial}{\partial \theta} \left(\sin \theta \frac{\partial}{\partial \theta} \right) \Phi(\theta, \phi) \\ &+ \frac{1}{\Phi(\theta, \phi)} \frac{1}{r^2 \sin^2 \theta} \frac{\partial^2}{\partial \phi^2} Y(\theta, \phi) = -\lambda_{n,k}^2, \end{aligned} \quad (\text{S24})$$

in which the first term of the equality only depends on time, the second term only depends on the radial and angular components, and then both should be equal to a constant $-\lambda_{n,k}^2$ chosen by convenience. Therefore, the time-dependent solution will be given by

$$\begin{aligned} \frac{1}{DT(t)} \frac{\partial}{\partial t} T(t) &= -\lambda_{n,k}^2 \\ T(t) &= C_1 \exp(-\lambda_{n,k}^2 Dt), \end{aligned} \quad (\text{S25})$$

NMR modes

where C_1 is a constant of integration. On the other hand, the radial and angular-dependent part leads to

$$\begin{aligned} \frac{1}{R(r)} \frac{\partial}{\partial r} \left(r^2 \frac{\partial}{\partial r} \right) R(r) + \lambda_{n,k}^2 r^2 = - \frac{1}{\Phi(\theta, \phi)} \frac{1}{\sin \theta} \frac{\partial}{\partial \theta} \left(\sin \theta \frac{\partial}{\partial \theta} \right) \Phi(\theta, \phi) \\ - \frac{1}{\Phi(\theta, \phi)} \frac{1}{\sin^2 \theta} \frac{\partial^2}{\partial \phi^2} \Phi(\theta, \phi) = n(n+1), \end{aligned} \quad (\text{S26})$$

in which the first term of the equality only depends on the radius, the second term only depends on the angular components, and then both should be equal to a constant $n(n+1)$ chosen for convenience. Hence, we get two separate equations. The angular equation

$$- \left(\frac{1}{\sin \theta} \frac{\partial}{\partial \theta} \left(\sin \theta \frac{\partial}{\partial \theta} \right) - \frac{1}{\sin^2 \theta} \frac{\partial^2}{\partial \phi^2} \right) \Phi(\theta, \phi) = n(n+1) \Phi(\theta, \phi), \quad (\text{S27})$$

has a solution already shown to be

$$\Phi(\theta, \phi) = \sum_{n=0}^{\infty} \sum_{m=-n}^n C_{n,m} Y_n^m(\theta, \phi). \quad (\text{S28})$$

The radial component equation is given by

$$\frac{\partial}{\partial r} \left(r^2 \frac{\partial}{\partial r} \right) R(r) = - [\lambda_{n,k}^2 r^2 - n(n+1)] R(r). \quad (\text{S29})$$

It is important to recognize that Eq. (S29) is a Sturm–Liouville equation with solution

$$R(r) = \sum_{n=0}^{\infty} \sum_{k=1}^{\infty} [D_{n,k} j_n(\lambda_{n,k} r) + E_{n,k} y_n(\lambda_{n,k} r)], \quad (\text{S30})$$

where $j_n(\lambda_{n,k} r)$ and $y_n(\lambda_{n,k} r)$ are the n^{th} -order spherical Bessel function of the first and second kind, respectively. In order to satisfy the Neumann boundary conditions, and having in mind the result from Eq. (S30), we should obey

$$\begin{aligned} D_{n,k} \lambda_{n,k} j_n'(\lambda_{n,k} r_i) + E_{n,k} \lambda_{n,k} y_n'(\lambda_{n,k} r_i) &= 0, \\ D_{n,k} \lambda_{n,k} j_n'(\lambda_{n,k} r_f) + E_{n,k} \lambda_{n,k} y_n'(\lambda_{n,k} r_f) &= 0, \end{aligned} \quad (\text{S31})$$

from where we conclude that the only possible values of $\lambda_{n,k}$ are those that satisfy the determinant

$$\begin{aligned} \begin{vmatrix} j_n'(\lambda_{n,k} r_i) & y_n'(\lambda_{n,k} r_i) \\ j_n'(\lambda_{n,k} r_f) & y_n'(\lambda_{n,k} r_f) \end{vmatrix} &= 0, \\ j_n'(\lambda_{n,k} r_i) y_n'(\lambda_{n,k} r_f) - y_n'(\lambda_{n,k} r_i) j_n'(\lambda_{n,k} r_f) &= 0. \end{aligned} \quad (\text{S32})$$

Thus, the eigenvalues $\lambda_{2,k}$ will be the positive roots of Eq. (S32), such that the solution will be expanded in terms of their corresponding eigenfunctions. Here, we ignore the the trivial solution $\lambda_{n,k} = 0$.

Because of the impenetrability condition given by $R'(0) = 0$, all $E_{n,k}$ coefficients are zero since the spherical Bessel functions of the second-kind $y_n(r)$ does not obey that condition (the solution blows up when $r_i \rightarrow 0$). Finally, the solution for $\rho(r, \theta, \phi, t)$ is given by

$$\rho(\mathbf{r}, t) = \sum_{n=0}^{\infty} \sum_{m=-n}^n \sum_{k=1}^{\infty} F_{n,m,k} j_n(\lambda_{n,k} r) Y_n^m(\theta, \phi) \exp(-\lambda_{n,k}^2 D t) \quad (\text{S33})$$

in which the coefficients $F_{n,m,k}$ are the combination (product) of all the previous coefficients for each separable solution, and they depend on the initial condition $\rho(\mathbf{r}, 0)$ as

$$F_{n,m,k} = \frac{\int_0^{2\pi} \int_0^{\pi} \int_{r_i}^{r_f} \rho(\mathbf{r}, 0) j_n(\lambda_{n,k} r) Y_n^m(\theta, \phi) r^2 \sin \theta d\theta d\phi}{\int_0^{2\pi} \int_0^{\pi} \int_{r_i}^{r_f} |j_n(\lambda_{n,k} r) Y_n^m(\theta, \phi)|^2 r^2 \sin \theta d\theta d\phi}. \quad (\text{S34})$$

The initial distribution of the system is given by the delta functions at a initial configuration $\{r_0, \theta_0, \phi_0\}$ and the corresponding closure relationships, i.e.,

$$\begin{aligned} \rho(\mathbf{r}, 0) &= \frac{\delta(r - r_0) \delta(\theta - \theta_0) \delta(\phi - \phi_0)}{r^2 \sin \theta} p(\mathbf{r}_0) \\ &= p(\mathbf{r}_0) \sum_{n=0}^{\infty} \sum_{m=-n}^n \sum_{k=1}^{\infty} Y_n^{m*}(\theta, \phi) Y_n^m(\theta_0, \phi_0) \frac{j_n(\lambda_{n,k} r) j_n(\lambda_{n,k} r_0)}{N_{n,k}}, \end{aligned} \quad (\text{S35})$$

in which the normalization constant (for Neumann boundary conditions) is given by

$$\begin{aligned} N_{n,k} &= \int_{r_i}^{r_f} j_n(\lambda_{n,k} r) j_n(\lambda_{n,k} r) r^2 dr = \\ &= \frac{r_f^3}{2} \left(1 - \frac{n(n+1)}{(r_f \lambda_{n,k})^2} \right) j_n(\lambda_{n,k} r_f) - \frac{r_i^3}{2} \left(1 - \frac{n(n+1)}{(r_i \lambda_{n,k})^2} \right) j_n(\lambda_{n,k} r_i). \end{aligned} \quad (\text{S36})$$

The probability $p(r_0, \theta_0, \phi_0)$ of having the initial condition configuration at equilibrium is given by

$$\begin{aligned} p(\mathbf{r}_0) &= \frac{p(r_0) p(\theta_0) p(\phi_0)}{r_0^2 \sin \theta_0} \\ &= \frac{1}{r_0^2 \sin \theta_0} \frac{r_0^2}{\int_{r_i}^{r_f} r^2 dr} \frac{\sin \theta_0}{\int_0^{\pi} \sin \theta d\theta} \frac{1}{\int_0^{2\pi} d\phi} \\ &= \frac{3}{4\pi(r_f^3 - r_i^3)}, \end{aligned} \quad (\text{S37})$$

such that

$$\rho(\mathbf{r}, 0) = \frac{3}{4\pi(r_f^3 - r_i^3)} \sum_{n=0}^{\infty} \sum_{m=-n}^n \sum_{k=1}^{\infty} Y_n^{m*}(\theta, \phi) Y_n^m(\theta_0, \phi_0) \frac{j_n(\xi_{n,k} r) j_n(\xi_{n,k} r_0)}{N_{n,k}}. \quad (\text{S38})$$

NMR modes

In NMR relaxation, we are only interested in the second moment ($n = 2$), and we will also assume that the system is isotropic ($m = 0$). Thus, the general solution $\rho(\mathbf{r}, t)$ simplifies to

$$\rho(\mathbf{r}, t) = \sum_{k=1}^{\infty} F_{2,0,k} j_2(\lambda_{2,k} r) Y_2^0(\theta, \phi) \exp(-\lambda_{2,k}^2 D t), \quad (\text{S39})$$

with the corresponding initial condition

$$\rho(\mathbf{r}, 0) = \frac{3}{4\pi(r_f^3 - r_i^3)} \sum_{k=1}^{\infty} Y_2^{0*}(\theta, \phi) Y_2^0(\theta_0, \phi_0) \frac{j_2(\lambda_{2,k} r) j_2(\lambda_{2,k} r_0)}{N_{2,k}}. \quad (\text{S40})$$

Thus, the coefficients are given by

$$F_{2,0,k} = \frac{\int_0^{2\pi} \int_0^\pi \int_{r_i}^{r_f} \rho(\mathbf{r}, 0) j_2(\lambda_{2,k} r) Y_2^0(\theta, \phi) r^2 \sin \theta d\theta d\phi}{\int_0^{2\pi} \int_0^\pi \int_{r_i}^{r_f} |j_2(\lambda_{2,k} r) Y_2^0(\theta, \phi)|^2 r^2 \sin \theta d\theta d\phi}. \quad (\text{S41})$$

Considering the orthogonality relationship of spherical harmonics and spherical Bessel functions, the coefficients of the solution will be given by

$$\begin{aligned} F_{2,0,k} &= \frac{3Y_2^0(\theta_0, \phi_0)}{2\pi r_f^6} \frac{\int_0^{2\pi} \int_0^\pi Y_2^0(\theta, \phi) Y_2^{0*}(\theta, \phi) \sin \theta d\theta d\phi \int_{r_i}^{r_f} r^2 j_2(\lambda_{2,k} r) \sum_{i=1}^{\infty} \frac{j_2(\xi_{2,i} r) j_2(\xi_{2,i} r_0)}{N_{2,i}} dr}{\int_0^{2\pi} \int_0^\pi |Y_2^0(\theta, \phi)|^2 \sin \theta d\theta d\phi \int_{r_i}^{r_f} |j_2(\lambda_{2,k} r)|^2 r^2 dr} \\ &= \frac{3Y_2^0(\theta_0, \phi_0)}{2\pi r_f^6} \frac{\sum_{i=1}^{\infty} \frac{j_2(\xi_{2,i} r_0)}{N_{2,i}} \int_{r_i}^{r_f} j_2(\lambda_{2,k} r) j_2(\xi_{2,i} r) r^2 dr}{\int_{r_i}^{r_f} |j_2(\lambda_{2,k} r)|^2 r^2 dr} \\ &= \frac{3}{4\pi(r_f^3 - r_i^3)} \frac{Y_2^0(\theta_0, \phi_0) j_2(\lambda_{2,k} r_0)}{N_{2,k}}. \end{aligned} \quad (\text{S42})$$

The final solution to the time-dependent equilibrium distribution probability between the two dipoles undergoing NMR relaxation at constant distance is given by

$$\rho(\mathbf{r}, t) = \frac{3}{4\pi(r_f^3 - r_i^3)} Y_2^0(\theta_0, \phi_0) Y_2^0(\theta, \phi) \sum_{k=1}^{\infty} \frac{j_2(\lambda_{2,k} r_0)}{N_{2,k}} j_2(\lambda_{2,k} r) \exp(-\lambda_{2,k}^2 D t). \quad (\text{S43})$$

Using this result in Eq. (5) and integrating over all possible coordinates in the system, we find that

$$\begin{aligned} G(t) &= \frac{4\pi}{5} \left(\frac{\mu_0}{4\pi} \right)^2 \hbar^2 \gamma_I^2 \gamma_S^2 S(S+1) \frac{3}{4\pi(r_f^3 - r_i^3)} \\ &\int_0^{2\pi} \int_0^\pi Y_2^0(\theta_0, \phi_0) Y_2^0(\theta, \phi) \sin \theta d\theta d\phi \int_0^{2\pi} \int_0^\pi Y_2^{0*}(\theta, \phi) Y_2^0(\theta, \phi) \sin \theta d\theta d\phi \quad (\text{S44}) \\ &\int_{r_i}^{r_f} \int_{r_i}^{r_f} \sum_{k=1}^{\infty} r^2 \frac{1}{r^3} r_0^2 \frac{1}{r_0^3} \exp(-\lambda_{2,k}^2 D t) \frac{j_2(\lambda_{2,k} r) j_2(\lambda_{2,k} r_0)}{N_{2,k}} dr dr_0, \end{aligned}$$

NMR modes

and by the orthogonality of the spherical harmonics, we obtain that

$$G(t) = \left(\frac{\mu_0}{4\pi}\right)^2 \hbar^2 \gamma_I^2 \gamma_S^2 S(S+1) \frac{3}{5(r_f^3 - r_i^3)} \sum_{k=1}^{\infty} \exp(-\lambda_{2,k}^2 Dt) \int_{r_i}^{r_f} \int_{r_i}^{r_f} \frac{1}{rr_0} \frac{j_2(\lambda_{2,k}r) j_2(\lambda_{2,k}r_0)}{N_{2,k}} dr dr_0. \quad (\text{S45})$$

Observe that now the NMR autocorrelation function has a multi-exponential decay over an infinite set of discrete characteristic decay times. It is important to emphasize that the quantity in Eq. (S45) should be computed under the definition of the inner-product (orthogonality) in Eq. (S36) that arise from the boundary conditions, such that the calculated quantities are projected into the correct orthogonal eigenvector space.

C. Padé-Laplace inversion of $G(t)$

In this section, we present the NMR dipole-dipole autocorrelation function $G(t)$ from MD simulations and the corresponding reconstruction of the signal using the Padé-Laplace inversion method through the captured modes. Figure S1 and S2 compile the reduced NMR dipole-dipole autocorrelation functions for two dipoles at different fixed distances (and constant friction) and for different frictions rates (and constant distance), respectively. Figure S3 shows the reduced NMR dipole-dipole autocorrelation functions for the case of a dipole diffusing on a thick spherical shell around the first dipole, for different reduced inner radius r_i . Overall, we observe very good agreement between the original autocorrelation functions from MD simulations and the corresponding reconstructed signal using the Padé-Laplace inversion method. Notice that the autocorrelation functions from MD simulations present noise, which increases with time. On the other hand, the reconstructed signal from the captured modes is smooth and only contains the exponential contributions obtained through the Padé-Laplace inversion (no noise).

NMR modes

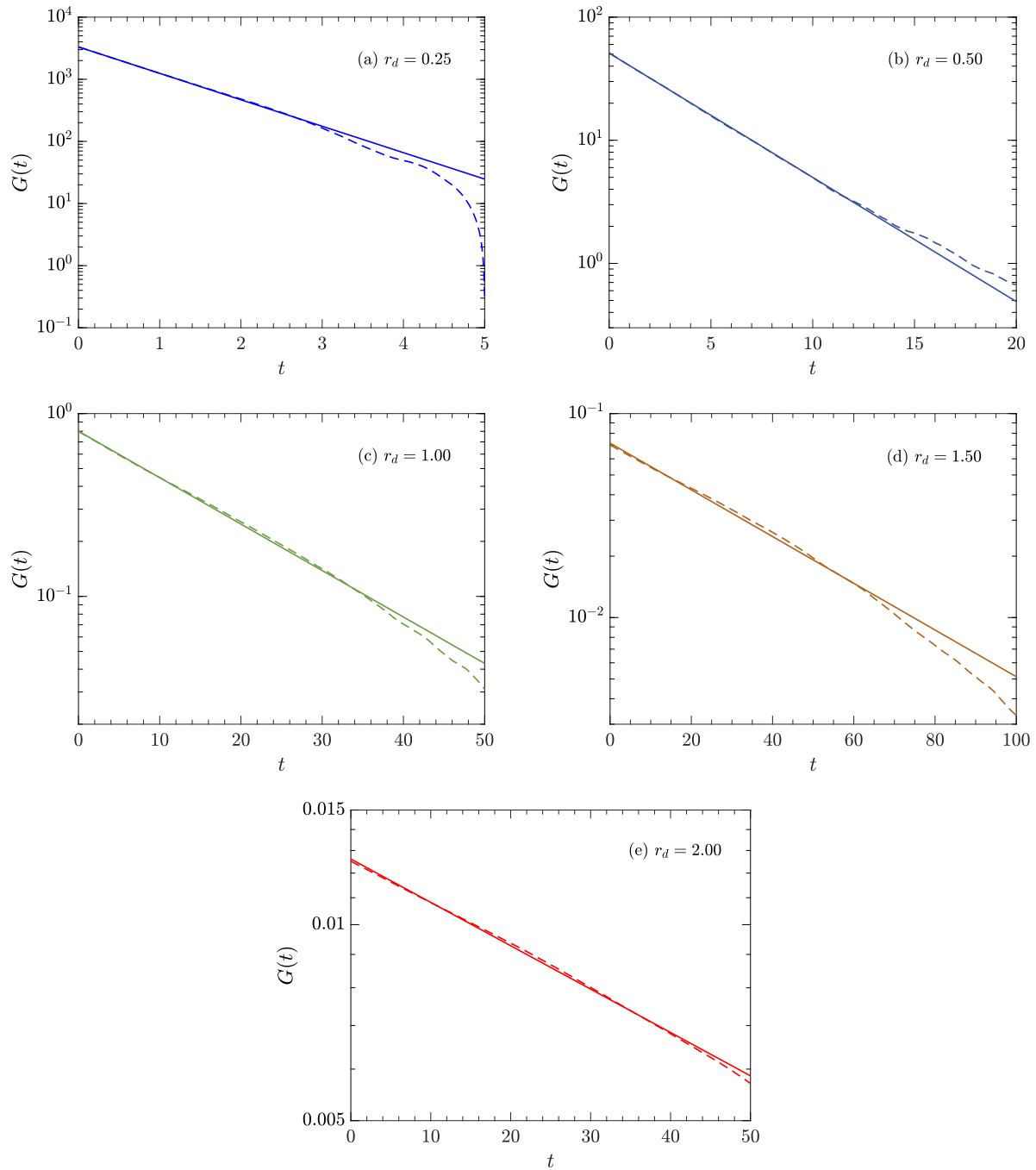


FIG. S1. Reduced NMR dipole-dipole autocorrelation function between two dipoles for difference fixed distances r_d , with $f = 10$ and $T = 1.00$. The dashed lines represent the MD simulation results, while the solid lines represent the reconstruction of the signal given by the Padé-Laplace inversion method.

NMR modes

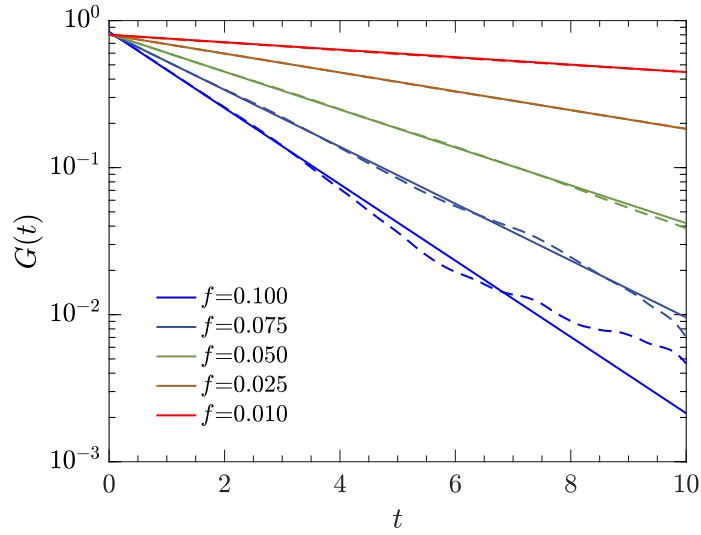


FIG. S2. Reduced NMR dipole-dipole autocorrelation function between two dipoles at a fixed distance $r_d = 1.00$ and with different friction constants f , with $T = 1.00$. The dashed lines represent the MD simulation results, while the solid lines represent the reconstruction of the signal given by the Padé-Laplace inversion method.

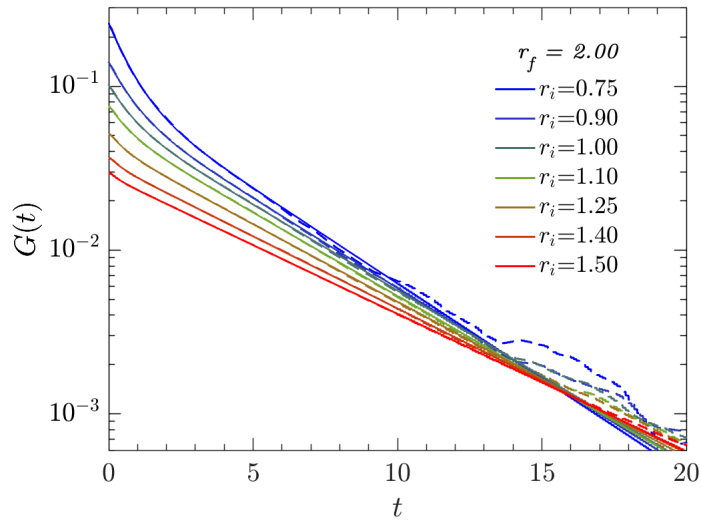


FIG. S3. Reduced NMR dipole-dipole autocorrelation function between two dipoles with the second one diffusing on a thick spherical shell, for different values of inner radius r_i and with $r_f = 2.00$, $f = 10$, and $T = 1.00$. The dashed lines represent the MD simulation results, while the solid lines represent the reconstruction of the signal given by the Padé-Laplace inversion method.

D. Numerical approximations for integral computations

When computing the result in Eq. (S45), we have to observe that the inner-product definition is not the regular Euclidean definition commonly used in algebraic calculations and software packages. Observe that such integrals should be strictly evaluated in a non-Euclidean space respecting the inner-product definition (orthogonality) given by Eq. (S36), which arises from the reflective boundary conditions.

For the particular problem under investigation, we observed that for the first molecular mode ($k = 1$) the orthogonality integral evaluated with the Euclidean inner-product definition is approximately the same as the analytical evaluation in the corresponding non-Euclidean space, within less than 5% numerical deviation across $0 < r_i/r_f < 1$. Hence, it is expected that numerical errors for the computation of the integral in Eq. (S45) (to which no analytical solution is available) due to deviations from the non-Euclidean inner-product will be negligible. However, for higher order molecular modes ($k \geq 2$), the deviations of the inner-product integral from the Euclidean definition with respect to the exact non-Euclidean computation is not negligible (above 5% in relative error) for certain values of r_i/r_f , and hence so will the quantity in Eq. (S45) if computed with the regular Euclidean inner-product. Figure S4 shows the relative error in the orthogonality condition integrals between using the Euclidean inner-product and the analytical solution (non-Euclidean solution), for different molecular modes and across the entire range of r_i/r_f and with $r_f = 2.00$.

To by-pass this limitation, and having in mind that no analytical solution to the integration to Eq. (S45) in the corresponding non-Euclidean space is available, we have computed the integrals using the regular inner product definition for the cases where the relative deviation on the orthogonality condition was less than 5%. When this error becomes greater than that, we did not compute the integrations numerically. However, given that the deviation is oscillatory and we are able to compute the integrals for points before and after high error regions, we can interpolate the curve with a smooth function, represented through dotted lines in our plots. This is a valid argument since the actual solution is expected to be monotonic. Figure S5 shows the points where the integration is numerically accurate (deviation below 5%), and the corresponding interpolation curve. For simplicity, after a certain point, we only included the interpolation curve in the paper plots. We highlight, however, that there are accurate data points in the dotted interpolation region to support the proposed trend.

NMR modes

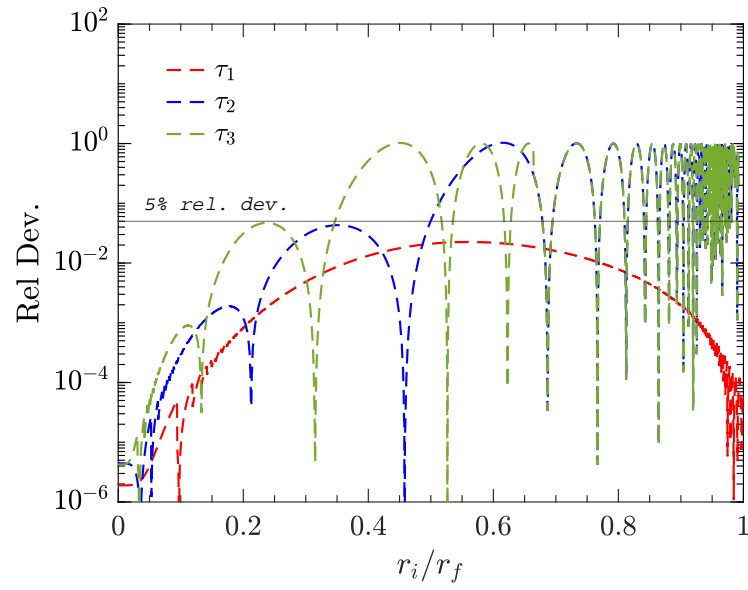


FIG. S4. Relative deviation on the computation of the orthogonality integral (Eq. (S36)) using the regular Euclidean inner-product and the non-Euclidean inner-product defined by the boundary conditions, across r_i/r_f and with $r_f = 2.00$.

NMR modes

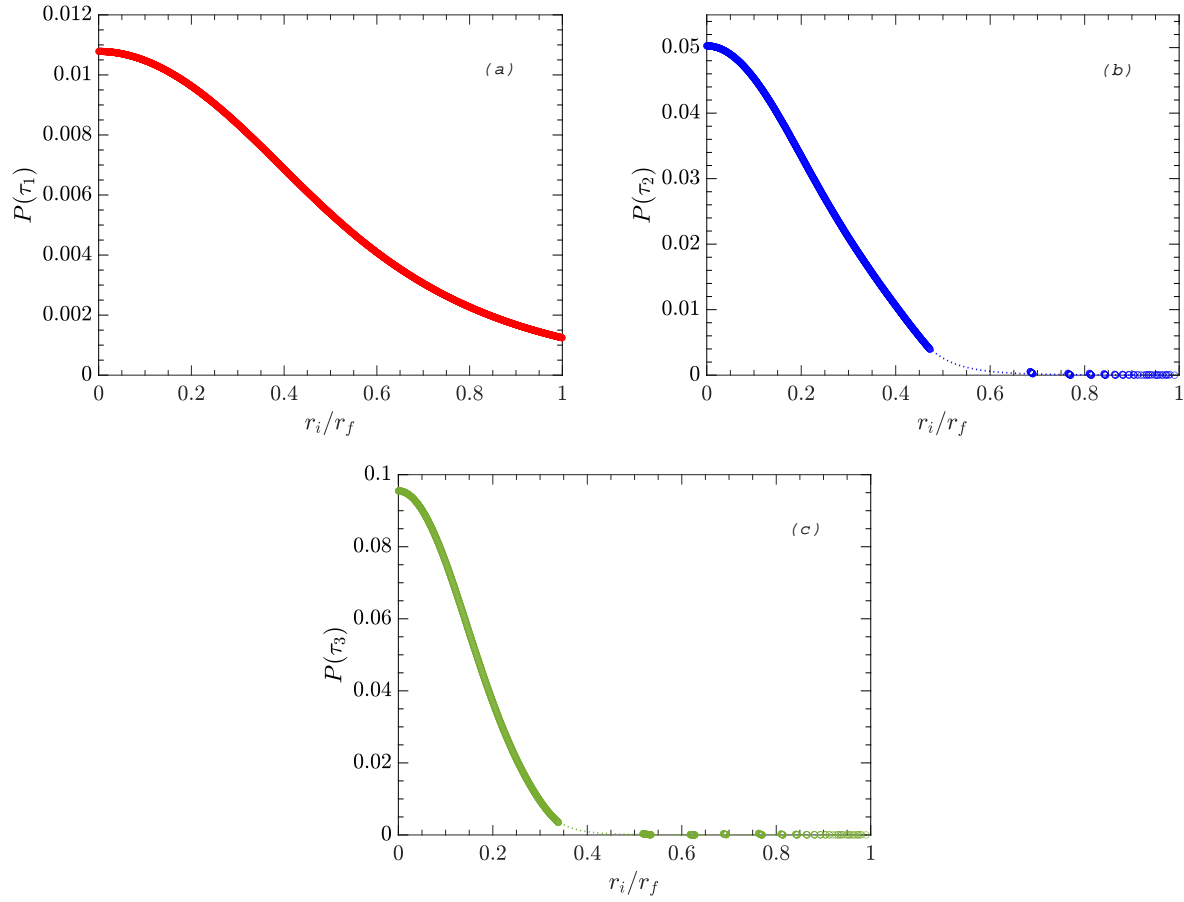


FIG. S5. Molecular modes reduced amplitudes $P(\tau_k)$ for the (a) first, (b) second, and (c) third modes across r_i/r_f , for the case of $r_f = 2.00$ with $f = 10$ and $T = 1.0$. The circle symbols represent the theoretical predictions using the regular Euclidean inner-product but with relative error in the orthogonality integral below 5%, while the dotted lines are the smooth interpolation of the theoretical predictions.

E. Molecular modes via theory and MD simulations

The raw data for the molecular modes obtained by both our theory and MD simulations are presented in Tables I, II, and III for the cases of different constant radii r_d , $r_i/r_f = 0.375$, and $r_i/r_f = 0.550$, respectively.

TABLE I. Molecular modes of NMR relaxation in LJ-reduced units for dipole pairs at different fixed distances r_d , with constant friction $f = 100$ and $T = 1.00$

r_d	τ		$P(\tau)$	
	Theory	MD simulations	Theory	MD simulations
0.25	1.04	1.02	3.259E+02	3.300E+02
0.50	4.17	4.30	5.093E+00	5.070E+00
1.00	16.67	17.09	7.958E-02	7.969E-02
1.50	37.50	37.93	6.986E-03	7.162E-03
2.00	66.67	65.19	1.243E-03	1.255E-03

TABLE II. Molecular modes of NMR relaxation in LJ-reduced units for dipole pairs at non-fixed distances for the case of $r_i = 0.75$ and $r_f = 2.00$, with constant friction $f = 10$ and $T = 1.00$

k	τ_k		$P(\tau_k)$	
	Theory	MD simulations	Theory	MD simulations
1	3.72	3.74	7.246E-03	9.06E-03
2	0.81	0.73	1.306E-02	1.53E-02
3	0.32	–	1.590E-03	–
4	0.16	–	3.219E-04	–
5	0.09	–	7.147E-07	–

NMR modes

TABLE III. Molecular modes of NMR relaxation in LJ-reduced units for dipole pairs at non-fixed distances for the case of $r_i = 1.10$ and $r_f = 2.00$, with constant friction $f = 10$ and $T = 1.00$

k	τ_k		$P(\tau_k)$	
	Theory	MD simulations	Theory	MD simulations
1	4.20	4.26	4.701E-03	5.48E-03
2	0.62	0.66	1.192E-03	2.18E-03
3	0.19	0.15	5.946E-05	1.37E-07
4	0.09	–	1.879E-05	–
5	0.05	–	1.296E-05	–

F. Mode contributions to relaxation dispersion

Figure S6 shows the theoretical percentage contribution to the relaxation rate $1/T_{1,2}$ at zero frequency ($\omega_0 = 0$) from different molecular modes of relaxation, over a certain range of r_i/r_f . The contribution to $1/T_{1,2}$ at $\omega_0 = 0$ from the k^{th} -mode is proportional to $P(\tau_k)\tau_k$. Observe that the first mode dominates $1/T_{1,2}$ at $\omega_0 = 0$ above $r_i/r_f \gtrsim 0.6$, and tends to 100% at $r_i/r_f = 1$ (i.e., in the BPP limit).

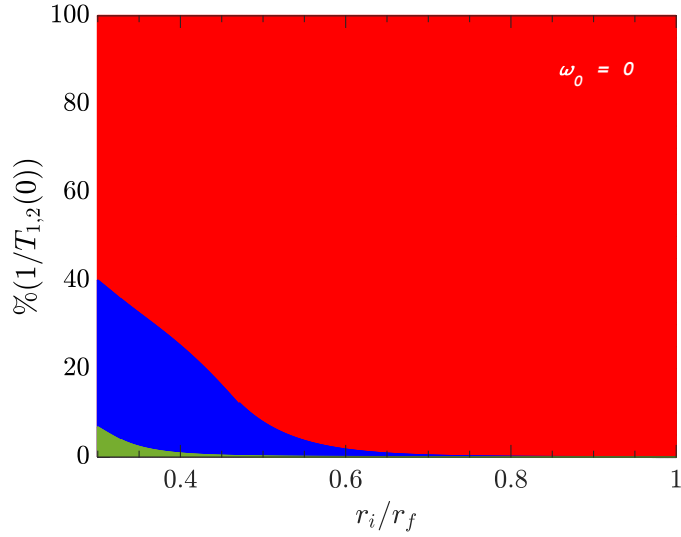


FIG. S6. Percentage theoretical contribution to $1/T_{1,2}$ at $\omega_0 = 0$ from the first molecular mode (red), second mode (blue), and third mode (green).

We can also estimate the mode contributions to $1/T_1(\omega_0)$ dispersion (i.e., as a function of frequency) for like spins, such that⁵:

$$\frac{1}{T_1(\omega_0)} = 2 \sum_k P(\tau_k) \left[\frac{\tau_k}{1 + (\omega_0 \tau_k)^2} + \frac{4\tau_k}{1 + (2\omega_0 \tau_k)^2} \right]. \quad (\text{S46})$$

Figures S7 and S8 show the theoretical percentage contribution from different molecular modes to $1/T_1(\omega_0)$ assuming two like-spin particles at $\omega_0 = 1/\tau_d = 0.15$ and $\omega_0 = 2/\tau_d = 0.30$, respectively, over a certain range of r_i/r_f with $r_f = 2.00$. Observe that as ω_0 increases, the relative importance of higher order modes ($k \geq 2$) to $1/T_1(\omega_0)$ also increases.

Meanwhile $1/T_2(\omega_0)$ shows only minor dispersion.

NMR modes

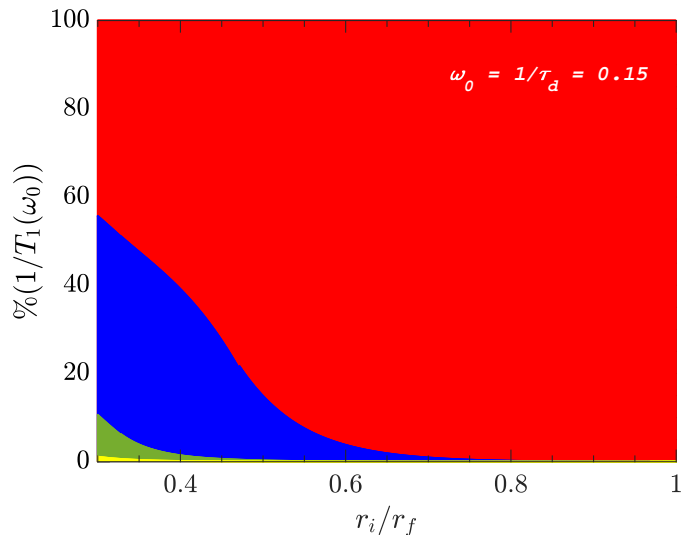


FIG. S7. Percentage theoretical contribution to $1/T_1(\omega_0)$ at $\omega_0 = 1/\tau_d = 0.15$ that arise from the first molecular mode (red), second mode (blue), third mode (green), and fourth mode (yellow), with $r_f = 2.00$. Within this range of r_i/r_f , the contribution of high order modes is negligible.

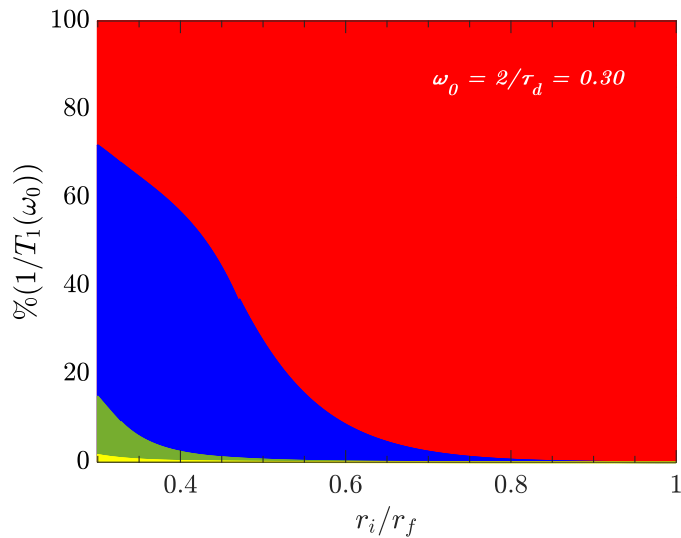


FIG. S8. Percentage theoretical contribution to $1/T_1(\omega_0)$ at $\omega_0 = 2/\tau_d = 0.30$ that arise from the first molecular mode (red), second mode (blue), third mode (green), and fourth mode (yellow), with $r_f = 2.00$. Within this range of r_i/r_f , the contribution of high order modes is negligible.

NMR modes

Note that for the case of unlike spins, the equivalent expression can be determined as such⁶

$$\frac{1}{T_1(\omega_0)} = 2 \sum_k P(\tau_k) \left[\frac{\tau_k}{1 + (\omega_0 \tau_k)^2} + \frac{7/3 \tau_k}{1 + (\omega_e \tau_k)^2} \right], \quad (\text{S47})$$

where $\omega_e = 658\omega_0$ is the resonance frequency of the electron spin.

REFERENCES

¹From the closure relationship of spherical harmonics, we know that

$$\frac{\delta(\theta - \theta_0)\delta(\phi - \phi_0)}{\sin \theta} = \sum_{n=0}^{\infty} \sum_{m=-n}^n Y_n^{m*}(\theta, \phi) Y_n^m(\theta_0, \phi_0) \quad (\text{S48})$$

.

²From the orthogonality relationship of spherical harmonics, we know that

$$\int_0^{2\pi} \int_0^{\pi} Y_n^m(\theta, \phi) Y_n^{m*}(\theta, \phi) \sin \theta d\theta d\phi = \delta_{n,n} \delta_{m,m}. \quad (\text{S49})$$

.

³B. J. Berne and R. Pecora, *Dynamic light scattering with applications to chemistry, biology, and physics*, 1st ed., Vol. 1 (John Wiley & Sons, Inc., 2000).

⁴N. Bloembergen and L. O. Morgan, “Proton relaxation times in paramagnetic solutions. Effects of electron spin relaxation,” *The Journal of Chemical Physics* **34**, 842–850 (1961).

⁵A. Valiya Parambathu, W. G. Chapman, G. J. Hirasaki, D. Asthagiri, and P. M. Singer, “Effect of nanoconfinement on NMR relaxation of heptane in kerogen from molecular simulations and measurements,” *Journal of Physical Chemistry Letters* **14** (4), 1059–1065 (2023).

⁶T. J. Pinheiro dos Santos, A. V. Parambathu, C. C. Fraenza, C. Walsh, S. G. Greenbaum, W. G. Chapman, D. Asthagiri, and P. M. Singer, “Thermal and concentration effects on ¹H NMR relaxation of Gd³⁺-aqua using MD simulations and measurements,” *Physical Chemistry Chemical Physics* **24**, 27964–27975 (2022).